Co-channel Digital Signal Separation: Application and Practice

by

Dawei Shen

Submitted to the Program in Media Arts and Sciences, School of Architecture and Planning
in partial fulfillment of the requirements for the degree of

Master of Science in Media Arts and Sciences

at the

MASSACHUSETTS INSTITUTE OF TECHNOLOGY

February 2008

Author .....
Program in Media Arts and Sciences
January 18, 2008

Certified by .....
Andrew B. Lippman
Senior Research Scientist of Media Arts and Sciences
Thesis Supervisor

Accepted by .....
Deb Roy
Chairman, Departmental Committee on Graduate Students

Co-channel Digital Signal Separation: Application and Practice

by

Dawei Shen

Submitted to the Program in Media Arts and Sciences, School of Architecture and Planning
on January 18, 2008, in partial fulfillment of the
requirements for the degree of
Master of Science in Media Arts and Sciences

Abstract

This thesis studies the theory and application of co-channel digital signal separation techniques. We set up a test-bed with the GNU Software Defined Radio (SDR) platform where we implement and experiment with single-antenna signal separation algorithms. We mainly investigate linearly-modulated digital signals. To do this, we design a multiple RFID card reader capable of decoding multiple commodity ID cards simultaneously. These passive RFID cards transmit DBPSK waveforms once activated. A signal separation function at the receiver delivers great convenience to the users without increasing the complexity and cost of the cards. Second, we derive the optimal criteria for deciding the start of an RFID frame. We show that the commonly utilized correlation rule is suboptimal and that a correction term needs to be considered to achieve the best detection performance. Several rules for frame synchronization are proposed and analyzed numerically using Monte Carlo simualtion. These signal separation techniques present an opportunity to improve the capacity of wireless systems and combat interference. This thesis documents design issues in the physical and application layers, thereby demonstrating the great flexibility and strength of the GNU SDR system.

Thesis Supervisor: Andrew B. Lippman
Title: Senior Research Scientist of Media Arts and Sciences

Co-channel Digital Signal Separation: Application and Practice

Date of Submission:

January 18, 2008

THESIS ADVISOR: Dr. Andrew B. Lippman
Senior Research Scientist of Media Arts and Sciences
MIT Media Lab

SIGNED: _____

THESIS READER: Dr. David P. Reed
Adjunct Professor of Media Arts and Sciences
MIT Media Lab

SIGNED: _____

THESIS READER: Dr. Dina Katabi
Associate Professor of Electrical Engineering and Computer Science
Computer Science and Artificial Intelligence Laboratory

SIGNED: _____

Acknowledgments

Thanks to my advisors Andy and David for their ideas, guidance and support. Thanks to the incredible building - MIT E15. Since I came to the media lab, I have been deeply impressed and influenced by creative faculty members and students. Their ideas and demonstrations have inspired me to see how human-beings social lives may be combined with technology seamlessly. I feel so proud to be a member of this family.

Thanks to Dina for spending her time discussing with me, reading and commenting on my work.

Thanks to my parents and Liwen for their endless love and support.

Thanks to my labmates: Grace, Kwan, Hector, Pol, Nadav, Fulu and Sung for their help and encouragement. I am so fortunate to be working with you.

Thanks to all my friends!

"Still have enough to pay for your food? Then, never give up" - My dad told me

Contents

List of Figures

Chapter 1

Introduction

1.1 Motivation

The cocktail party effect describes the human's exceptional ability to listen to a single speaker among a mixture of conversations and background noises [3]. In a very noisy party, we can still listen and understand what our friend says while simultaneously ignoring what nearby people are saying. If another friend far away suddenly calls our names, we can still recognize the sound and respond quickly. Interestingly, engineers have not developed communication devices with such amazing auditory capabilities. Figure.1-1 compares these two scenarios.

Consider the case of having multiple RFID cards coexisting in our wallet. In order to open a door protected by an RFID reader, we usually have to flip the wallet for several times in front of the reader or even take the correct card out. All the cards transmit RF signals interfering with each other. However, the reader only responds to the loudest one or simply chooses to stay confused. A more sophisticated system bypasses this problem by avoiding simultaneous transmissions by using smarter, but more costly RFID cards. An immediate question is: why don't we enable the receiver to separate and decode multiple signals, so that the other parts of the system remain unchanged and users can enjoy the convenience?

Figure 1-1 – A cocktail party versus a communication network, where a receiver is not capable of decoding simultaneously transmitted signals

In a wireless network system, if multiple signals coexist in the same channel, undesired signals are considered as interference to the primary signal. Therefore, communication devices must be regulated to share the channel. The current solution generally adopts time-division multiplexing (TDM), frequency-division multiplexing (FDM) or code-division multiplexing (CDM). The multiplexing divides the channel into several orthogonal logical channels. Such practice requires precise coordination and timing synchronization. In a random access network such as today's Wi-Fi networks, simultaneously transmitted packets lead to a collision. Both packets are discarded and retransmissions must be made later. Intuitively, a considerable amount of information is abandoned and wasted in conventional network settings. If sophisticated signal processing could enable us to jointly decode concurrently transmitted signals with high reliability, it is expected that the capacity of wireless networks can be effectively improved and higher layer protocols can be optimally redesigned.

1.2 Significance

Digital signal separation has wide applications in cellular networks and RFID systems which are presented in this thesis. More importantly, it provides us with a new perspective on the design and analysis of future ad-hoc network systems, and leads us to rethink how we deal with interference.

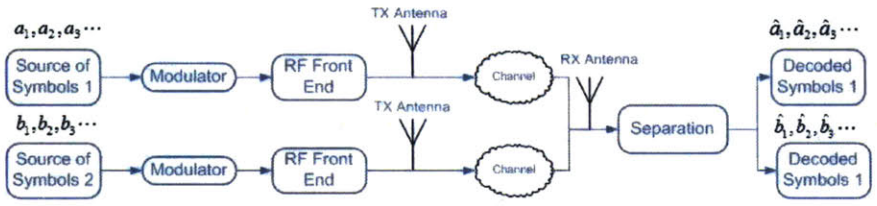

Figure 1-2 – A simplified channel model of digital signal separation. Two transmitters are sending signals to the same receiver at the same time.

In cellular networks, the dominant channel impairment is co-channel interference (CCI), introduced by frequency reusage. Advanced signal processing techniques can be applied to the receiver to mitigate the effects caused by the interfering signals and noise. In today's Wi-Fi networks, the medium access control (MAC) layer assumes simple collision models, i.e., collisions among users mainly cause the failure of packet delivery. The basic approach to improve the MAC's performance is to resolve collisions by limiting transmissions. Conventional MAC protocols, especially for random access ad-hoc networks, suffer from hidden terminal problems, which severely limit the effectiveness of techniques based on carrier sensing. Digital signal separation apparently provides an alternative way to solve the hidden terminal problem. Furthermore, if the receiver has the multipacket reception capability, the MAC layer protocol should encourage, rather than limit, simultaneous transmissions of users to improve the throughput of the network[18].

In this thesis, we study the theory and application of co-channel digital signal separation techniques. We set up a test-bed with the GNU Software Defined Radio (GNU SDR, or GNU Radio) platform, on which we implement and experiment with single-antenna signal separation algorithms.

First, we design a multiple RFID cards' reader, which is capable of reading and decoding multiple MIT student ID cards simultaneously. These passive RFID cards transmit DBPSK waveforms once they get activated. By enabling signal separation capability at the receiver, we deliver great convenience and efficiency to the users without increasing the complexity and cost of the cards.

Second, We derive the optimal criteria for deciding the start of an RFID frame, commonly known as the optimum frame synchronization problem, for multiple access channels. Due to its important theoretical value, we devote a standalone chapter to this topic.

We document design issues we have encountered in physical and application layers, thereby demonstrating the great flexibility and strength of the GNU Radio system. Data will be processed online and offline in GNU Radio to analyze the effects and evaluate the performance.

1.3 Contributions

The main contributions of the work discussed in this thesis include:

1. We implement a complete multiple RFID card reader, capable of decoding signals emitted by simultaneously activated RFID tags. Compared with the previous work on multiple RFID decoding presented in [20], our work exhibits significant improvements in many aspects:

    - Our extendible algorithm is capable of reading more cards than the method introduced in [20], which handles only two cards. The design and analysis presented in this thesis is mostly based on four cards. However, the number of cards that can be successfully decoded is only constrained by the computational power and the amount of memory used in the software radio system, not the algorithm itself.
    - The reader we implement runs in real time and delivers the identity information embedded in the cards with little processing delay.
    - We estimate the power levels of the received signal by using a histogram of the received samples, and then calculate the amplitudes of the transmitted signals by solving a set of linear equations according to the least square error criteria. This approach provides very accurate estimates of the signal

amplitudes. In contrast, [20] uses a simple approach to estimate signal amplitudes, which usually leads to incorrect detection due to its inaccuracy. Additionally, the approach used in [20] can not be extended.

2. We study the problem of optimum frame synchronization for multiple access channels (MAC). While Massey [15] and several following researchers have discovered the optimal criteria for frame detection in point-to-point channels, few research efforts have been made for multiple access channels, especially for the frame-asynchronous case. In this thesis, we present new research results for both frame-synchronous and frame-asynchronous cases. We show that the optimal rule for frame detection in multiple access channels adds a correction term to the correlation term. When multiple transmitters are present, Gaussian approximation can be used to simplify the decoding rule.

1.4 Structure

In the next chapter, we summarize the relevant background materials on co-channel digital signal separation. We will survey existing algorithms and discuss their usabilities. We also introduce the fundamental principles of the GNU Radio platform and the RFID system. Chapter 3 documents a detailed process of designing a multiple RFID card reader. We discuss design decisions and present numerical results in this chapter. The optimum frame synchronization algorithm for locating the starting sample of an RFID frame is derived in Chapter 4. We demonstrate that the optimum decision rule we develop outperforms the simple correlation rule we used to utilize. We introduce our future research on signal separation algorithms for GMSK modulation in Chapter 5 for both synchronous and asynchronous cases. Finally, in Chapter 6, we make some concluding remarks and suggest areas of further research.

Chapter 2

Background

2.1 Relevant Research Work

Co-channel signal separation techniques have been developed by researchers mainly as tools to alleviate co-channel interference (CCI) encountered in cellular networks and other communication systems. Many proposed algorithms stem from interference cancellation/suppression techniques and adaptive equalizing methods. Though tremendous research efforts have been focused on utilizing antenna arrays instead of one single receive antenna, multiple antennas usually lead to costly and complex receivers with unacceptable sizes. Therefore, a single antenna system is an attractive option, which is also the focus of this thesis.

Generally speaking, digital waveforms employed today can be categorized into two classes according to their different modulation schemes: linear modulation (MPSK/QAM, e.g.) and constant envelop modulation (GMSK/MSK, e.g.)[2]. In linear modulation, a symbol is mapped to a complex point of a constellion on a 2-dimensional plane. These complex symbols then pass through a pulse-shaping function block, which, coupled with a match filter at the receiver, is designed to relieve inter-symbol interference (ISI) effects caused by the wireless channel. The impact of the channel on the signal is usually modelled as an FIR filter with complex-valued taps or the so-called

channel coefficients. With regard to constant envelop modulation, the amplitude of a sample at any time instant is unvarying. The digital information is embraced inside the phase, or more precisely, the instantaneous frequency of the signal. Over the past decade, various co-channel signal separation methods have been proposed for different modulation schemes under different assumptions.

2.1.1 Algorithms for Linear Modulation Schemes

For linear modulation schemes, a series of nonlinear methods based on joint maximum likelihood sequence estimation (JMLSE) were proposed in [7, 5, 6]. These literatures have an in-depth and thorough treatment of the optimal joint estimator of two co-channel linearly modulated signals. In [7], a suboptimal, joint MAP symbol detection (JMAPSD) algorithm based on a Bayesian recursion was proposed. Good estimates of the primary and secondary signal powers are assumed to be available a-priori. The channel coefficients are assumed to be known for both JMLSE and JMAPSD. Alternatively, they can be estimated blindly, which leads to joint blind MAP co-channel symbol detector (JBMAPSD). Besides Giridhar's outstanding work, a conventional independent component analysis (ICA) approach to blindly separate MPSK signals is described in [19]. A quasi-linear demod-remod system for recovering co-channel QAM signals in the presence of ISI was proposed in [9]. Accurate estimation of channel coefficients plays a crucial role and the study in [10] addresses a pilot-based MMSE technique for multiuser channel estimation in a TDMA system.

2.1.2 Algorithms for Constant Envelop Modulation Schemes

For constant envelop modulation such as GMSK, the demod-remod technique is an attractive option for its conceptual simplicity and low design complexity [8]. Algorithms based upon JMLSE were discussed and analyzed in [16, 17]. Both papers assume GMSK signals must be transmitted synchronously. If we treat continuous-phase frequency shift keying (CPFSK) signals as ordinary FM signals, then techniques

for analog FM signal separation could also be brought into the picture. Hamkins compared three approaches in his work: cross-coupled phase locked loop (CCPLL) method, joint Viterbi algorithm, and an analytic technique [11], which we will study and test extensively in the thesis. All three methods are built upon the same idea: jointly tracking the phases of the two waveforms since the digital information is carried in the instantaneous frequencies of the signals. This is an effective approach because it doesn't require symbol-level synchronization between the two sources and the knowledge of training sequences is not necessary at the receiver. Besides, this method is robust to carrier frequency offsets. However, we have to transmit packets continuously from the two sources to make them behave like analog FM signals. In [12], the joint estimation problem is formulated using state space equations and the estimator structure is derived based on the extended Kalman filter (EKF).

2.2 GNU Software Defined Radio

Most algorithms introduced above have been only validated via mathematical proofs or computer simulation. Few of them provide convincing results for real-world, over-the-air data. Most importantly, some methods are developed based on assumptions which are hardly realizable in practice or usable with existing hardware. For example, some methods require accurate estimation of channel coefficients and signal power, while some methods rely on the synchronization of two packets. We usually meet unexpected obstacles and challenges when we implement these ideas in real systems and test the algorithms using data that come through a real wireless channel.

GNU Software Defined Radio, together with its hardware counterpart, the Universal Software Radio Peripheral (USRP) board, provides an ideal test-bed for experimenting with these new techniques. 'GNU Radio is a free software toolkit for learning about, building, and deploying software defined radios'. GNU Radio takes what is traditionally done in hardware and brings it into software, providing great convenience and flexibility for academic users. Reconfigurability is the key feature[4].

The USRP board is the associated hardware counterpart specifically designed by Ettus for GNU Radio use[1]. The USRP main board contains four 64 MS/s 12-bit analog-to-digital converters(ADC), and four 128 MS/s 14-bit digital-to-analog converters (DAC). The USRP board exchanges samples with the computer via a high-speed USB 2.0 interface. Due to the limitation of the USB bus, the USRP is only capable of processing signals with bandwidths of up to 16 MHz. Various daughter boards are available covering various frequency bands between 0 and 2.9 GHz.

At this stage, we have a stable functional DBPSK, GMSK and OFDM implemented and carefully tested in the GNU Radio code base. Despite certain limitations imposed by the current architecture of GNU Radio, we can readily build our signal separation program based on the existing signal processing modules. One shortcoming is that GNU Radio doesn't support feedback flows from one block back to another block.

2.3 RFID Systems

Radio frequency identification (RFID) is an automatic identification method using devices including RFID tags and readers. An RFID tag contains an antenna for receiving and transmitting signals, and an integrated circuit for storing and processing identification information. RFID tags can be roughly categorized into two types. Passive tags do not have internal power supply, i.e., the interal circuit can only be activated by incoming radio frequency signals. In contrast, active RFID tags have their own power sources and broadcast RF waves to readers. RFID systems work in different frequency bands: low frequency (LF, 125kHz), high frequency (HF, 13.56MHz) and ultra high frequency (UHF, 900MHz).

RFID technology has received remarkable attention in recent years. It has very broad applications in transportation payments, inventory control, product tracking, and people/animal identification. At the same time, it also has engendered considerable controversy on privacy concerns.

MIT deploys an RFID system on campus using Indala's products. All student ID cards are passive RFID tags working in the 125kHz band. If multiple ID cards appear in front of the reader, all of them will accumulate enough power from the carrier signal emitted by the reader, and start to transmit signals back to the reader. In such a situation, the reader may not be able to decode the desired identification signal. This motivates us to investigate signal separation methods to solve this problem.

Chapter 3

Design and Analysis of a Multiple RFID Card Reader

In this chapter, we present a complete system design of a multiple RFID card reader, which is implemented using the GNU Software Radio system. The reader is capable of decoding simultaneous RFID signals. We first introduce the basics of the RFID system deployed at MIT. Then, we model multiple RFID signals mathematically and formulate the separation problem as a maximum likelihood (ML) detection problem. We next describe the algorithm for estimating the power levels of the received signal and calculating the signal amplitudes from the estimated levels. Design parameters and their impacts on the decoding performance are then analyzed numerically. We demonstrate that the signal separation function at the receiver delivers great convenience to the users without increasing the complexity and cost of the cards.

3.1 Specification of MIT ID Cards

In this section, we introduce the basics of the MIT RFID card system that we work with. MIT deploys Indala Proximity 125kHz readers and compatible student ID cards on campus. The readers constantly generate 125kHz sine waves. When a

passive student RFID card approaches the reader, it gets activated after accumulating enough power. On the receiving end, the reader sees the 125 kHz carrier gets AM modulated by a 62.5 kHz signal. The bits are DBPSK encoded on the 62.5 kHz signal. A '1' corresponds to a phase shift and a '0' means no phase shift. Mathematically, the digital signal received by the reader when only one card is activated can be represented by

$$r(t) = (A + B(t)\cos(2\pi 62.5kt + \phi))\cos(2\pi 125kt + \theta). \tag{3.1}$$

A is the amplitude of the 125kHz carrier when no card is present. θ, ϕ are unknown, but correlated phase offsets. They satisfy the relationship:

$$\theta - 2\phi = 0 \quad \text{or} \pm \pi, \tag{3.2}$$

because the RFID card derives its clock from the external sine wave. All the RFID cards transmit signals that are synchronized with the carrier, with possible $0, \pm\pi/2, \pi$ ambiguities. $B(t)$, generated by the passive RFID card, is a None-Return-to-Zero (NRZ) DBPSK waveform containing the encoded binary information. Its time domain waveform is shown in Figure.3-3. $B(t)$ can be expressed by

$$B(t) = h\sum_k d_k a(t - kT), \tag{3.3}$$

where h is the amplitude representing the signal strength, $a(t)$ is a simple on-off square wave with a level of 1 when $0 < t \leq T$, and 0 elsewhere, d_k is a series of binary symbols valued from $1, -1$, differentially encoded. T is the symbol period. The symbol rate is $f_s = 125e3/32kHz \approx 3.91kHz$. $T = 1/f_s \approx 2.56 \cdot 10^{-4}$s.

Figure.3-1 shows the spectrum of the received signal $r(t)$ when an RFID tag is activated. Though the signal is expressed using continuous-time representation in Eq.(3.1) and Eq.(3.3), we process the signal discretely by first sampling the signal. The sampling rate we use is $f_s = 500$kHz. The strong peak at 125kHz is the carrier signal emitted by the reader. The two distinct lobes beside the peak, centered around

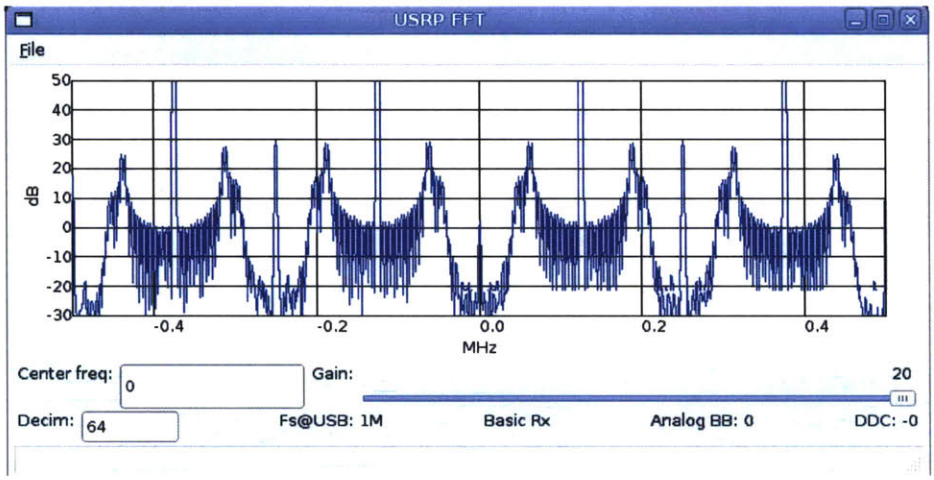

Figure 3-1 – The spectrum of the received signal $r(t)$ displayed using the Software Spectrum Analyzer provided by GNU Radio, one card is present, $f_s = 500\text{kHz}$

62.5kHz and 187.5kHz, exhibit the digital signals generated by the RFID tags. This can be explained by expanding $r(t)$ into three terms,

$$\begin{aligned} r(t) &= \frac{1}{2}B(t)\cos(2\pi 62.5kt + \phi - \theta) \\ &\quad + A \cdot \cos(2\pi 125kt + \theta) + \frac{1}{2}B(t)\cos(2\pi 187.5kt + \phi + \theta). \end{aligned} \tag{3.4}$$

Note that there are higher order harmonics visible in the spectrum, which are generated from the reader's circuitry. By using a band-pass FIR filter with cut-off frequencies of 20kHz and 105kHz, we remove the last two high frequency terms, retaining the information in $B(t)$,

$$r_0(t) = \frac{1}{2}B(t)\cos(2\pi f_0 t + \phi_0). \tag{3.5}$$

We can further decode the binary symbols from $r_0(t)$. The use of a band-pass filter guarantees that the DC component will also get removed. The spectrum of the resulting filtered signal is shown in Figure.3-2. The nominal value of f_0 is 62.5kHz. However, due to hardware limitation, there is usually a small frequency offset, which

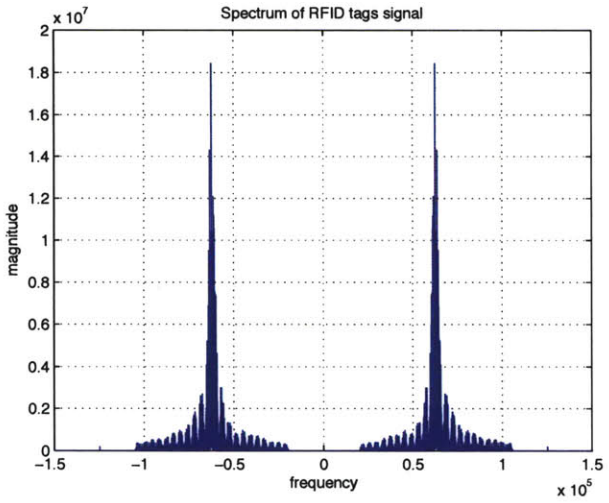

Figure 3-2 – The spectrum of $r_0(t)$, the output signal of the band-pass filter, centered at f_0 =62.5kHz, f_s=500kHz

must be estimated accurately. $\phi_0 = \phi - \theta$.

After recovering the carrier, $B(t)$ can be obtained by multiplying $r_0(t)$ with a cosine wave $\cos(2\pi f_0 t + \phi_0)$ that is locally generated (mixing). Then, we can low-pass filter the multiplied signal. This process is also called digital down conversion because the spectrum of the signal is moved from 62.5kHz down to 0Hz. Mathematically,

$$\begin{aligned} q_0(t) &= r_0(t)\cos(2\pi f_0 t + \phi_0) \\ &= \frac{1}{4}B(t) + \frac{1}{4}B(t)\cos(4\pi f_0 t + \phi_0) \\ p_0(t) &= \frac{1}{4}B(t). \end{aligned} \tag{3.6}$$

Finally, we obtain a square-shaped signal, $p_0(t) = B(t)$, with which we can directly decide digital information, as shown in Figure.3-3.

All the equations above use continuous-time representations. In a digital system, all signals are sampled by the analog-to-digital converter (ADC), and processed in the discrete domain. We set up the USRP board with a sampling rate of $f_s = 500$kHz. The symbol rate of the RFID signal is $f_{\text{sym}} = 125/32$kHz. Therefore, the oversampling rate for each symbol is $f_s/f_{\text{sym}} = 128$. Each MIT ID is uniquely identified with 224

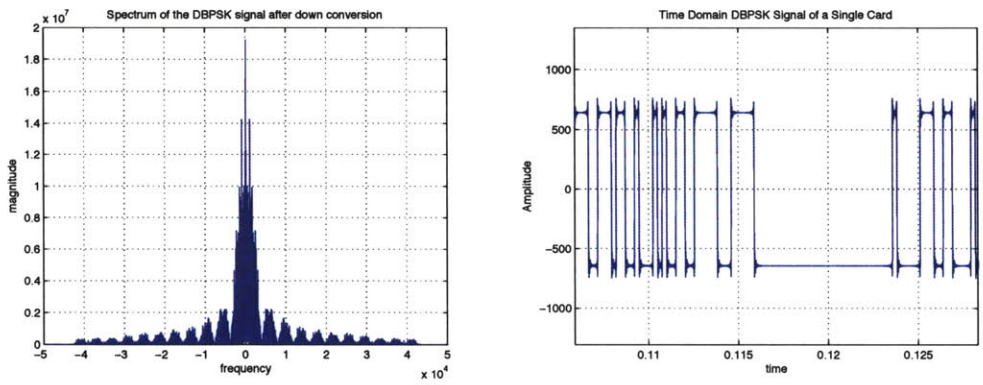

Figure 3-3 – The spectrum of $p_0(t) = 1/4B(t)$ (left) and its time domain waveform (right), only one card is activated, f_s=500kHz

bits, which we call a frame. Each frame starts with 30 zeros, which we can clearly observe from Figure.3-3. The RFID card, once activated, repeatly transmits the 224 bits over and over again. Interestingly, out of these 224 bits, only 32 vary among cards, all the other bits remain constant. This fact implies we can have as many as 192 bits as the sync-word when we try to locate an RFID frame. This important fact also helps us decode the information more reliably.

3.2 Channel Model for Multiple RFID Signals

When multiple cards come close to the reader, all of them may get activated and start transmitting signals back to the reader. There are several important facts we must be aware of in our system design.

First, cards usually get activated and start to transmit frames at different starting time instants. The timing offset between two signals must be a multiple of (1/125k) seconds (one period of the carrier). This is because RFID tags synthesize their internal clocks from the incoming 125kHz carrier, thus they transmit signals that are synchronized with the 125kHz sine wave. Second, because of the various distances between the cards and the reader, and also because of the nuances in hardware manufacturing, the signal strengths can be significantly different. This is a crucial factor

in being able to separate signals. Finally, all signals have the same center frequency f_0, but different phases ϕ_0, as shown in Eq.3.5. As introduced above, there can be a π or $\pi/2$ ambiguity between signals. This is another important factor in our system design. We will examine the effects of the phase offsets more carefully later.

The analysis above gives us the continuous-time channel model for multiple RFID signals:

$$r_0(t) = \sum_{l=1}^{N} B_l(t - \tau_l)\cos(2\pi f_0 t + \phi_0 + \theta_l) + n(t). \tag{3.7}$$

This channel model assumes the signal has been processed with the band-pass filter, but without down converting. Note that we still use $r_0(t)$, the same notation we used in Eq.(3.5), to denote the output signal of the band-pass filter. $n(t)$ is the additive white Gaussian noise. N is the number of activated cards. ϕ_0 is the unknown phase offset, as shown in Eq.(3.5). θ_l represents the phase ambiguity, which takes on values from $0, \pm\pi/2, \pi$. τ_l is the timing offset, which is a multiple of (1/125k) seconds . $B_l(t)$ has been given in Eq.(3.3), with the index l.

$$B_l(t) = h_l \sum_k d_{k,l} a(t - kT). \tag{3.8}$$

Figure.3-4 shows the block diagram of all pre-processing modules that process the received signal before we can apply the separation algorithm.

Because of the variance of the phase offsets among different signals, we cannot recover the phases of these signals using any conventional carrier synchronization approaches. In fact, the effects of the phase offsets can be reflected in the amplitudes after we down-convert the signal to 0-band. Remember that we down-convert a signal by low-pass filtering the mixing of $r_0(t)$ and a locally generated cosine wave.

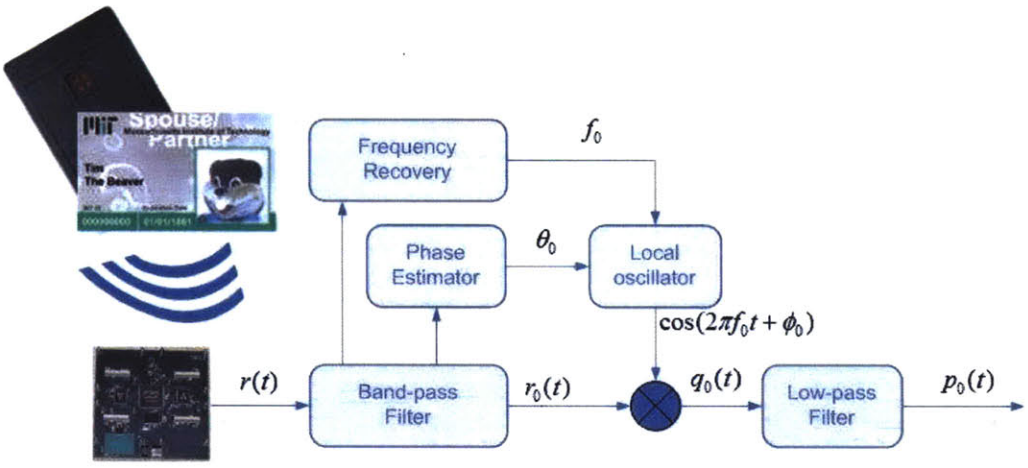

Figure 3-4 – The diagram of the modules that pre-process the RFID signal before the separation function block, which is implemented using GNU Radio

Mathematically, the output of the mixer is

$$\begin{aligned} q_0(t) &= r_0(t)\cos(2\pi f_0 t + \theta_0) \\ &= \left(\sum_{l=1}^{N} B_l(t-\tau_l)\cos(2\pi f_0 t + \phi_0 + \theta_l)\right)\cos(2\pi f_0 t + \theta_0) \\ &= \frac{1}{2}\sum_{l=1}^{N} B_l(t-\tau_l)\cos(\phi_0 + \theta_l - \theta_0) \\ &\quad + \frac{1}{2}\sum_{l=1}^{N} B_l(t-\tau_l)\cos(4\pi f_0 t + \phi_0 + \theta_l + \theta_0), \end{aligned} \tag{3.9}$$

where $\cos(2\pi f_0 t + \theta_0)$ is the cosine wave we generate locally. f_0 must be estimated accurately using frequency recovery techniques. θ_0 is only a design choice for us, and is not a parameter recovered from the received signal. We will discuss the selection of θ_0 in detail later. Note that here, we omit the noise term $n(t)$ for clarity. After low-pass filtering, we obtain:

$$p_0(t) = \frac{1}{2}\sum_{l=1}^{N} B_l(t-\tau_l)\cos(\phi_0 + \theta_l - \theta_0). \tag{3.10}$$

The 'cos' terms caused by phase shifts, $\cos(\phi_0 + \theta_l - \theta_0)$, become a scaling fac-

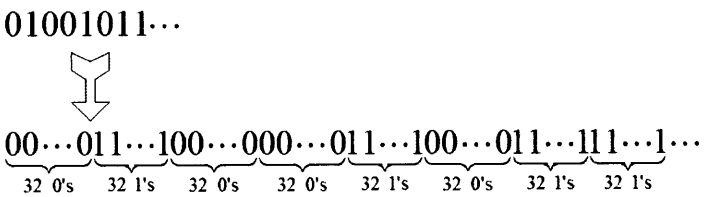

Figure 3-5 – Each symbol is expanded into 32 identical symbols that are consecutive in time.

tor of $B_l(t)$, which can be incorporated into the amplitudes h_l inside $B_l(t)$, i.e. $g_l = 1/2h_l \cos(\phi_0 + \theta_l - \theta_0)$. Each $B_l(t)$ is a square-shaped signal as shown in Figure.3-3. τ_l must be multiples of (1/125k) seconds, which provides us with some degree of convenience. If each (1/125k) second is a unit time, the starting time of each RFID signal must be aligned with one of these units. The symbol rate of the DBPSK signal is (125/32)kHz. We can split each symbol in time and treat it as 32 identical symbols. By doing this expansion, we achieve a higher symbol rate of 125kHz. More importantly, we achieve symbol level synchronization. Figure.3-5 explains this expansion.

The analysis above leads to a very succinct expression for the corresponding discrete-time channel model for multiple signals,

$$r[m] = \sum_{l=1}^{N} g_l \cdot d_l[m] + n[m]. \tag{3.11}$$

The $a(t)$ in Eq.(3.3) disappears in the equation since it only takes value from 0 or 1. g_l is the amplitude we calculated in the continuous-time channel model before. Here, we would like to incorporate the effects caused by different phase offsets. $d_l[m]$'s are ± 1 symbols. m here indexes the discrete samples. It has valid meanings in both 'sampling rate (500kHz)' indexes and 'expanded symbol rate (125kHz)' indexes. The difference is an oversampling factor of $f_s/f_{\text{esym}} = 4$. Since we are working with sampling-rate discrete signals, we assume m indexes the signal with the sampling rate. Note that in this case, each ± 1 symbol in the original packet is expanded into 128 samples.

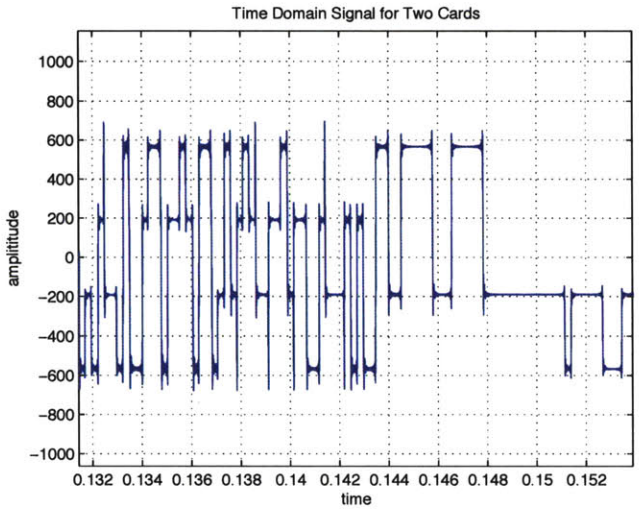

Figure 3-6 – The time-domain baseband discrete signal generated by two RFID cards (r[m]), sampled at f_s =500kHz, down-converted from 62.5kHz band to 0-band

Hence, the RFID signal separation problem can be summarized as: given $r[m]$, how can we decode $d_{k,l}$'s in Eq.(3.8) reliably?

3.3 RFID Signal Separation

3.3.1 Maximum Likelihood (ML) Detection

Let's consider the simplest case when only two cards are activated simultaneously. After band-pass filtering the signal, we obtain an accurate estimate of f_0 from $r_0(t)$ by using frequency recovery. With an appropriately chosen phase θ_0, we create a local cosine wave and mix it with the signal. Then, we obtain $r[m]$ by low-pass filtering the output of the mixer, whose time-domain waveform is displayed in Figure.3-6.

Compared with Figure.3-3, where only two power levels are present, Figure.3-6 demonstrates four different levels. We can understand this phenomenon from the

discrete channel model

$$r_2[m] = g_1 \cdot d_1[m] + g_2 \cdot d_2[m] + n[m]. \tag{3.12}$$

The subscript 2 is used to indicate the number of active signals. Without considering the noise term $n[m]$ and the Gibbs phenomenon caused by FIR filtering effects, there should be four different power levels existing if g_1 and g_2 are different, i.e.: $g_1+g_2, g_1-g_2, -g_1+g_2, -g_1-g_2$. Without loss of generality, we assume $g_1 > g_2 > 0$. This is clearly observable from Figure.3-6, where all samples are valued around $\pm 600, \pm 200$.

If we have estimated these four levels accurately (assuming they are $l_2, l_1, -l_1, -l_2$ and $l_2 > l_1 > 0$), we can further derive the values of g_1, g_2 into $g_1 = (l_2 + l_1)/2$ and $g_2 = (l_2 - l_1)/2$. The probability density function (pdf) of $r_2[m]$, given that $n[m]$ is white Gaussian noise is thus

$$p_{\mathbf{r}_2[m]}(r_2[m]) = \frac{1}{\sqrt{2\pi\sigma^2}} e^{-\frac{(r_2[m]-g_1 \cdot d_1[m]-g_2 \cdot d_2[m])^2}{2\sigma^2}}, \tag{3.13}$$

where σ^2 is the variance of the Gaussian noise.

Maximum likelihood (ML) detection is to find a pair $(d_1[m], d_2[m])$ from the four possible combinations, (1,1), (1,-1), (-1,1) and (-1,-1), such that the pdf in Eq.(3.13) is maximized. Equivalently, the distance between the received sample and the power level produced by $(d_1[m], d_2[m])$

$$|r_2[m] - g_1 \cdot d_1[m] - g_2 \cdot d_2[m]| \tag{3.14}$$

is minimized. In other words, we choose a pair that gives us a power level that is closest to $r_2[m]$. To further simplify the decision making process, we notice that the whole set of real numbers can be divided into four decision regions, which are separated by three thresholds: $g_1, 0$ and $-g_1$. We choose $(d_1[m], d_2[m])$ to be (1,1) if $r_2[m] > g_1$, (1,-1) if $0 < r_2[m] \leq g_1$, (-1,1) if $-g_1 < r_2[m] \leq 0$, and (-1,-1) if $r_2[m] \leq -g_1$.

The ML detection algorithm above presumes accurate estimates of the power levels, i.e., g_1 and g_2, are available. We will explore the estimation algorithm in subsequent subsections. Note that the ML detection algorithm can be easily extended to cases when more RFID cards' signals are present. For example, for the three cards' cases, the discrete channel model becomes

$$r_3[m] = g_1 \cdot d_1[m] + g_2 \cdot d_2[m] + g_3 \cdot d_3[m] + n[m]. \tag{3.15}$$

In this case, there are eight possible power levels:$g_1 + g_2 + g_3, g_1 + g_2 - g_3, g_1 - g_2 + g_3, g_1 - g_2 - g_3, -g_1 + g_2 + g_3, -g_1 + g_2 - g_3, -g_1 - g_2 + g_3, -g_1 - g_2 - g_3$. The ML detection rule is comparing $r_3[m]$ with seven thresholds and making a choice out of the eight possible states.

3.3.2 Estimation of Power Levels

In this subsection, we discuss how to estimate the distinct power levels. We are motivated by the fact that the power levels can be easily read from the probability density function(pdf) of the received samples. The location of the peaks (local maxima) are believed to be good estimates of the power levels. In our system design, we try to approximate the distribution by using a histogram of the samples, as shown in Figure.3-7.

In order to create the histogram, we divide the range of possible sample values into 1000 small bins and count the number of samples that fall into each bin. After obtaining the histogram, we perform peak detection in the histogram. By finding the local maxima, we locate where the signal power levels are. Finding these peaks can be done efficiently, we require that the number of samples in a bin must exceed a certain threshold and it must be larger than the counts for nearby bins.

We should emphasize that this approach of estimating the power levels is a good demonstration of the strength and flexibility provided by GNU Software Radio. In order to create the histogram of the samples, we need to buffer a large amount of

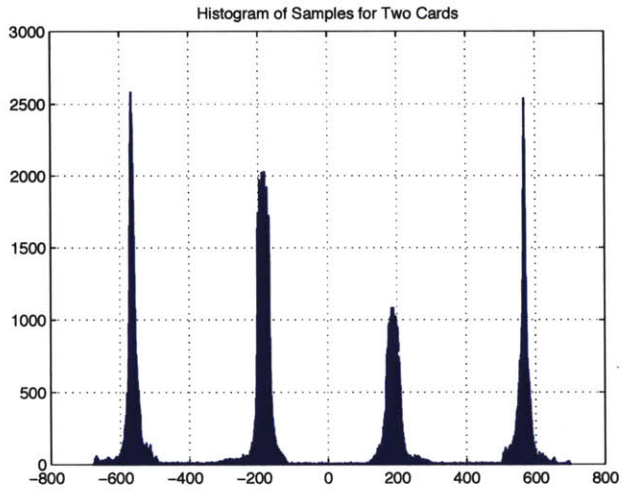

Figure 3-7 – The histogram of the discrete samples ($r_2[m]$) generated by two RFID cards, f_s=500kHz

data. The histogram in Figure.3-7 results from a collection of 200,000 samples. The requirement for a large amount of memory space is too demanding to be satisfied with most hardware implementation. However, software radio takes advantage of the convenience of software programming and the ease of memory allocation, making realization of our algorithm much simpler.

All peaks should be detected symmetrically, i.e., if l_k is the position of a peak representing a power level, $-l_k$ should be one too. This one degree of redundancy helps the peak detection become more robust.

In Figure.3-8 and Figure.3-9, we compare the time-domain waveforms and the histgrams of the samples for one, two, three and four card cases. The ML detection and power level estimation algorithms apply in the same way for the three and four card cases. For three cards, we can observe eight different signal levels, while four cards make 16 levels visible. Again, we emphasize that all peaks are symmetric. When we do peak detection, we must take this symmetry into account and choose from unwanted noisy peaks. For example, the peak detection in the four card case is

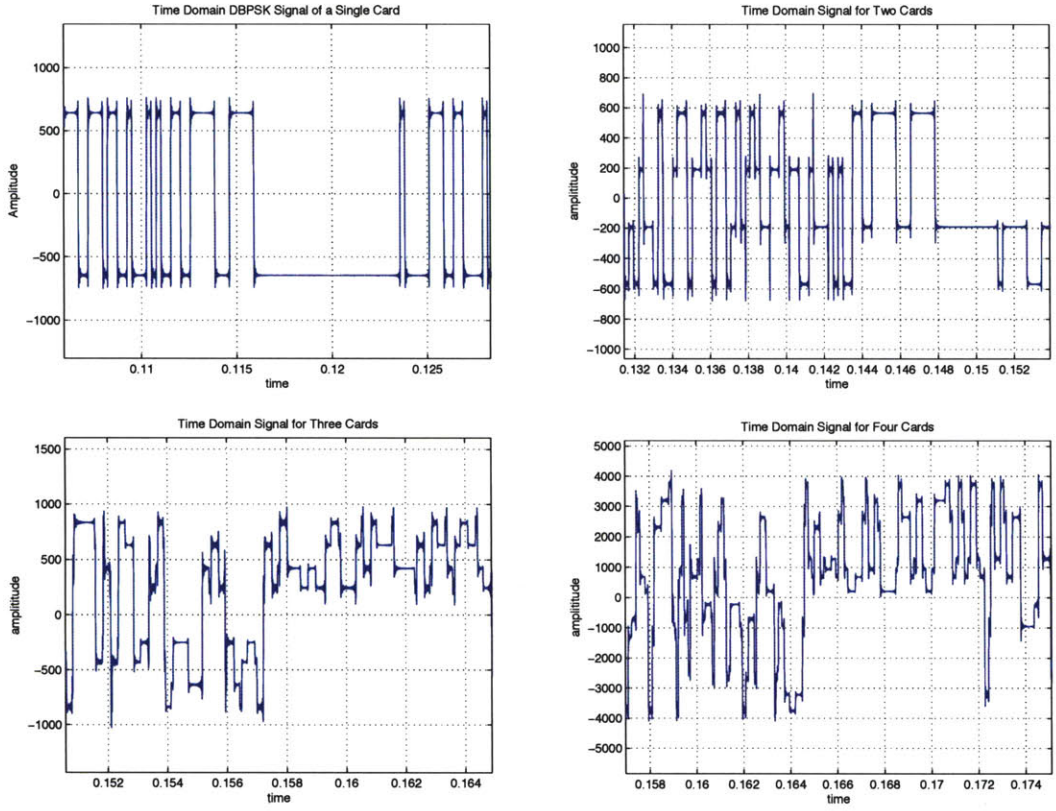

Figure 3-8 – The time domain baseband signals generated by one, two, three and four RFID cards, from which we can see 2, 4, 8 and 16 power levels respectively.

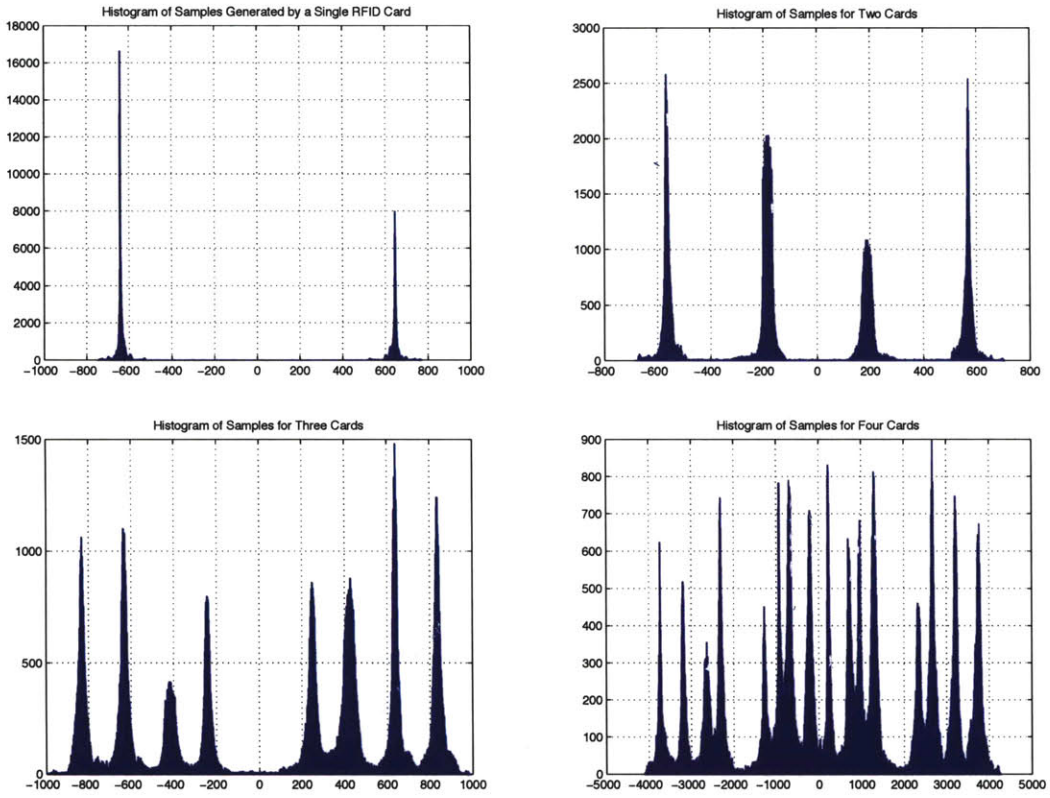

Figure 3-9 – The histogram of the discrete samples generated by one, two, three and four RFID cards, from which we can see 2, 4, 8 and 16 power levels respectively

shown in Figure.3-9 and returns the values:

$$l_8 = 3730 \quad l_7 = 3146 \quad l_6 = 2671 \quad l_5 = 2277$$
$$l_4 = 1332 \quad l_3 = 934 \quad l_2 = 744 \quad l_1 = 139$$

The negative power levels are symmetric to the positive power levels above, which are omitted here.

3.3.3 Calculating Amplitudes (g_l) from Power Levels

Peak detection provides us with 2^N different power levels. They are represented as $\pm l_1 \cdots \pm l_{2^{N-1}}$. Without loss of generality, we assume $0 < l_1 < l_2 < \cdots < l_{2^{N-1}}$. The thresholds used in the ML detection to determine decision regions are $(2^{N-1}-1)$ mid-points between every two adjacent levels. Next, we need to calculate the amplitudes $g_1, g_2, \cdots, g_N \quad (g_1 > g_2 > \cdots > g_N)$ from the power levels. In each decision region, we wish to select which combination of $(d_1[m], d_2[m], \cdots, d_N[m])$ gives the closed power level to $r_N[m]$. Such a decision can only be made with the knowledge of the values of the signal amplitudes.

For two cards, the computation is straightforward. $g_1 = (l_2+l_1)/2, g_2 = (l_2-l_1)/2$.

For three cards, it's a bit more complicated. $l_4 = g_1+g_2+g_3, l_3 = g_1+g_2-g_3, l_2 = g_1-g_2+g_3$. However, we can't decide whether $l_1 = g_1-g_2-g_3$ (when $g_1 > g_2+g_3$), or $l_1 = -g_1+g_2+g_3$ (when $g_1 < g_2+g_3$). This ambiguity doesn't bring too much trouble, because we have already got three equations while only three variables need to be solved. We can still calculate the values of g_1, g_2, g_3 without resolving the ambiguity. However, we should keep in mind that the values l_1, l_2, l_3, l_4 are obtained from peak detection in the histogram. This previous step is error prone. Additionally, introducing redundancy to the calculation only increases the robustness of the result if the extra complexity is still affordable by the computer. Therefore, a more systematic approach is to solve a series of linear equations using the least square error criteria

and to pick the one with the smallest error. Formulating the linear equations for the three cards' case, we have two possibilities:

$$\begin{pmatrix} 1 & 1 & 1 \\ 1 & 1 & -1 \\ 1 & -1 & 1 \\ 1 & -1 & -1 \end{pmatrix} \begin{pmatrix} g_1 \\ g_2 \\ g_3 \end{pmatrix} = \begin{pmatrix} l_4 \\ l_3 \\ l_2 \\ l_1 \end{pmatrix} \tag{3.16}$$

$$\begin{pmatrix} 1 & 1 & 1 \\ 1 & 1 & -1 \\ 1 & -1 & 1 \\ -1 & 1 & 1 \end{pmatrix} \begin{pmatrix} g_1 \\ g_2 \\ g_3 \end{pmatrix} = \begin{pmatrix} l_4 \\ l_3 \\ l_2 \\ l_1 \end{pmatrix} \tag{3.17}$$

For each set of linear equations, there are more equalities than unknown variables. Thus, we solve the equations using least square error criteria. We select the matrix that gives us the smallest square error. The solution vector $(g_1, g_2, g_3)'$ gives us the most accurate estimates of the amplitudes. At the same time, the lth row of the corresponding matrix tells us the symbols $(d_1[m], d_2[m], d_3[m])$ that we need to select if $r_3[m]$ falls into the lth decision region.

If we deal with more than four cards, there are more possible orders leading to more sets of linear equations to solve. This complexity increases exponentially with the number of cards. For example, for the four cards' case, we are only certain that $l_8 = g_1 + g_2 + g_3 + g_4$, $l_7 = g_1 + g_2 + g_3 - g_4$, and $l_6 = g_1 + g_2 - g_3 + g_4$. All the other levels can not be uniquely determined. We show in the appendix that there are 14 possible sets of linear equations we need to solve and to compare the square error.

One possible set of linear equations can be formulated as

$$\begin{pmatrix} 1 & 1 & 1 & 1 \\ 1 & 1 & 1 & -1 \\ 1 & 1 & -1 & 1 \\ 1 & 1 & -1 & -1 \\ 1 & -1 & 1 & 1 \\ 1 & -1 & 1 & -1 \\ 1 & -1 & -1 & 1 \\ 1 & -1 & -1 & -1 \end{pmatrix} \begin{pmatrix} g_1 \\ g_2 \\ g_3 \\ g_4 \end{pmatrix} = \begin{pmatrix} l_8 \\ l_7 \\ l_6 \\ l_5 \\ l_4 \\ l_3 \\ l_2 \\ l_1 \end{pmatrix}. \tag{3.18}$$

For example, for the four cards' case shown in Figure.3-9, we solve 14 sets of linear equations. The matrix above gives us the least square error. The four amplitudes are solved as

$$g_1 = 1877.78, \quad g_2 = 1078.16, \quad g_3 = 407.75, \quad g_4 = 241.47$$

The lth row of the matrix in Eq.(3.18) gives us the decoded bits if the received sample $r_4[m]$ falls in the lth decision region.

3.3.4 Frequency Estimation and Phase Selection

For estimating the frequency f_0 shown in Eq.(3.5), we use the direct FFT method described in [13]. The details are omitted here. We have mentioned in previous sections that there is no necessity for phase recovery in our algorithm because signals from different RFID cards have phase ambiguities among them. Therefore, the choice of θ_0 in reconstructing the local carrier is only a design choice. However, this greatly affects the performance of the power level detection and the overall effectiveness of our separation algorithm.

The key point in our design is that the algorithm relies on whether the peaks

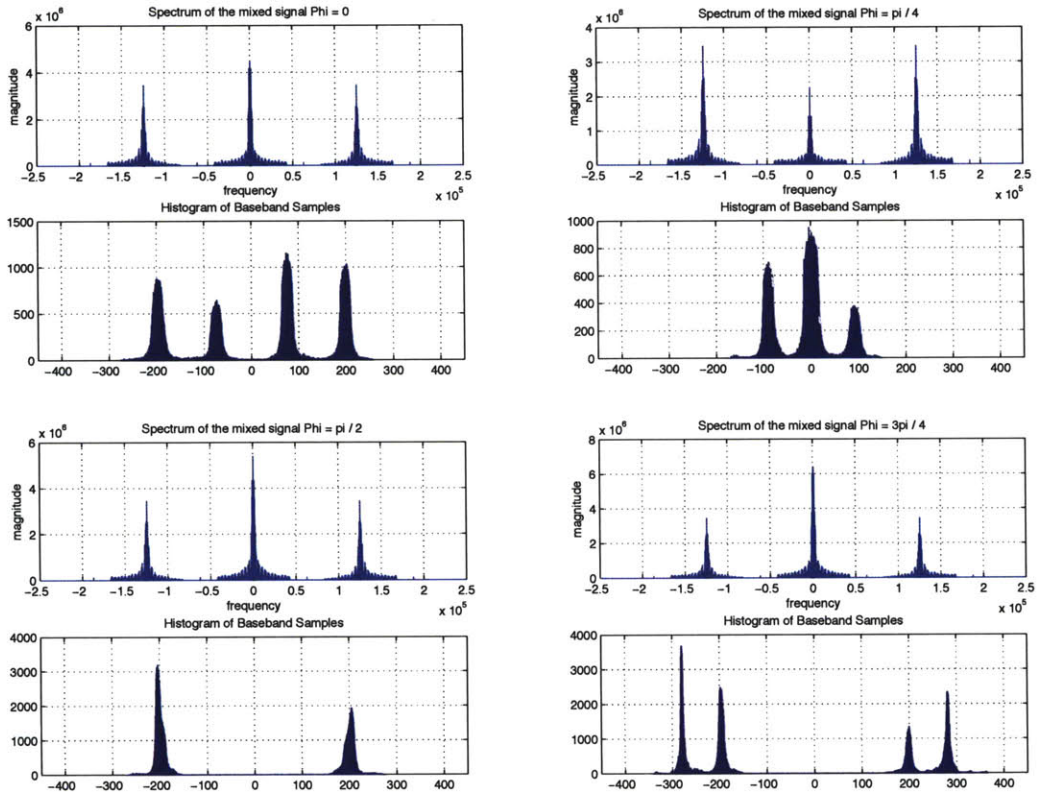

Figure 3-10 – The spectrum of the mixed signal $q_0(t)$ (above) and the histogram of the samples of the baseband signal ($r_2[m]$) generated by two cards (bottom), with $\theta_0 = 0, \pi/4, \pi/2, 3\pi/4$

in the histogram can be easily differentiated. This requirement in turn implies that the amplitudes of different signals $(g_1, g_2, \cdots)$ must be significantly different. From Eq.(3.10), we can perceive that the choice of θ_0 has a direct impact on whether we can achieve this goal. Figure.3-10 demonstrates the impact of choosing different values of θ_0 on the histogram for the received samples for the two cards' case. Four values of θ_0 are used to generate the local cosine wave: $0, \pi/4, \pi/2, 3\pi/4$. It's evident from the figure that the choice of θ_0 directly affects our ability to separate the peaks. From this figure, we can see that when $\theta_0 = 0$ or $3\pi/4$, the separability is acceptable, albeit not optimal. For $\theta_0 = \pi/4$, the situation becomes much worse, which correponds to the $g_1 = g_2$ case. Instead of seeing four power levels in the histogram, we can see only three because two of them are cancelled to be zeros. The worst case happens

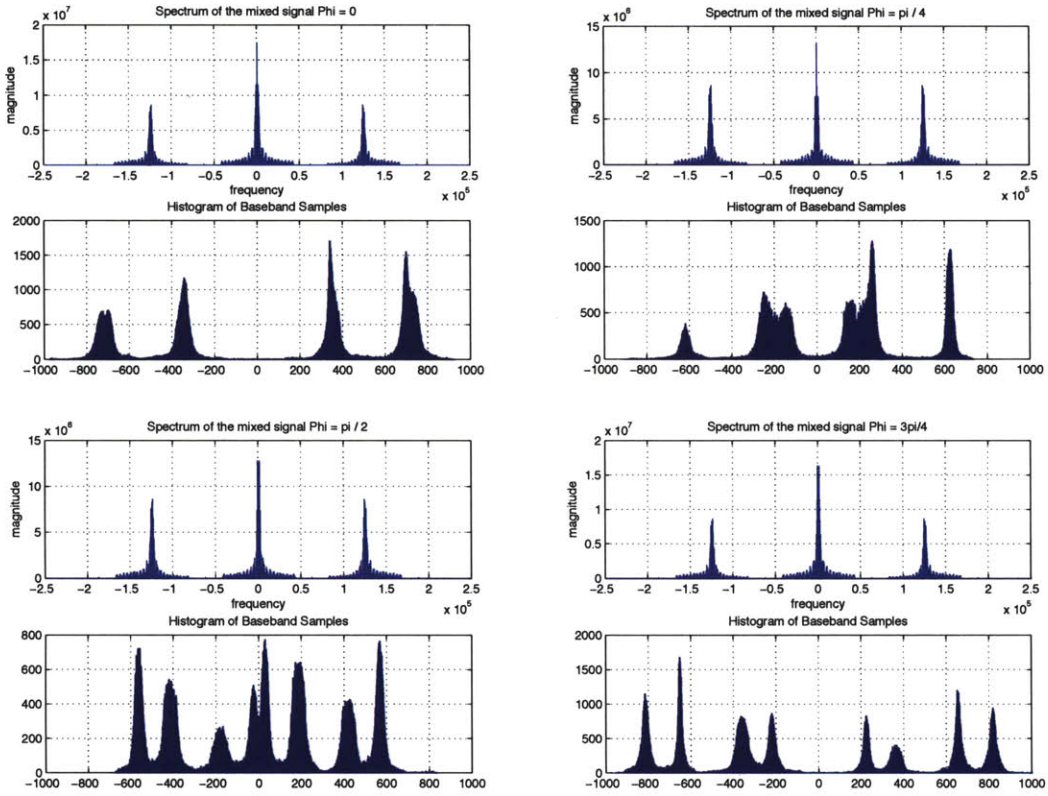

Figure 3-11 – The spectrum of the mixed signal $q_0(t)$ (above) and the histogram of the samples of the baseband signal ($r_3[m]$) generated by three cards (bottom), with $\theta_0 = 0, \pi/4, \pi/2, 3\pi/4$

when $\theta_0 = \pi/2$. In this case, one signal completely vanishes. This corresponds to $g_2 = 0$. Only one card can be read. Figure.3-11 demonstrates the phase effects for three cards. Only when $\theta_0 = 3\pi/4$ are the peaks separable.

It is very important for us to judiciously select the value of θ_0 in order to have our separation algorithm work. The easiest solution, which actually works very well, is to step through all values of θ_0 from 0 to π, with a step size of $\pi/16$. Though this exhaustive search method works well, it's not an elegant solution, since it adds too much computational burden to the CPU.

In Figure.3-10 and Figure.3-11, the graphs above the histograms display the spectrum of the output of the mixer in Eq.(3.9), i.e. $q_0(t)$, for different choices of θ_0. The spectrum of a 62.5kHz-band signal, after its being multiplied by a 62.5kHz co-

sine wave, is moved to 0-band and 125kHz-band. Experiments tell us that the more power is concentrated to 0-band, i.e., the more power remains after the following low-pass filtering, the more easily can the power levels be distinguished.

3.3.5 Framing and Packetizing

At the previous step, for every sample $r_N[m]$, we decide a vector $d_1[m], \cdots, d_N[m]$ using the ML detection rule. Then, we can split it into N streams. This is where we achieve the RFID signal separation.

Finally, for each individual stream, we perform frame synchronization to locate the starting sample of a 224-bit packet. Note that all the bits are differentially modulated, but we can still decode it as a BPSK waveform. Frame synchronization can be achieved by correlating the signal with the header containing 30 zeros. For the MIT ID card system, only 32 bits vary, and the remaining constant 192 bits can serve as the synchronization header.

Frame synchronization, although seemingly straighforward and simple to achieve, is a classic research topic in communication theory. For continuously transmitted frames, Massey discovered that the traditional correlation rule, though works well in practice, is actually not optimal. An additional term has to be added to account for the correlation between symbols[15]. However, no research results on frame synchroniation for multiple signals have been presented so far. Due to its theoretical importance, we devote the whole Chapter 4 to this topic.

The sampling rate is 128 times the symbol rate. Each symbol in the original packet is expanded into 128 identical symbols. We can process the signal as if we are looking for the 224×128-length, bigger packets. Due to the Gibbs phenomenon and the transition time near symbol boundries, we allow a few bits to be corrupted. This won't affect our decoding performance since each bit is repeated for 128 times. A majority decision rule can be applied for each symbol. Another more standard approach is to apply a match filter with 128 all-one taps to each stream and then to

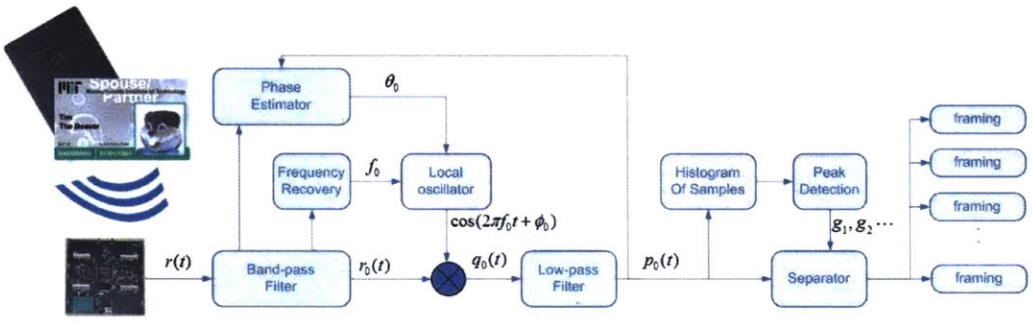

Figure 3-12 – The complete block diagram of the multiple RFID cards' reader, implemented using GNU Radio

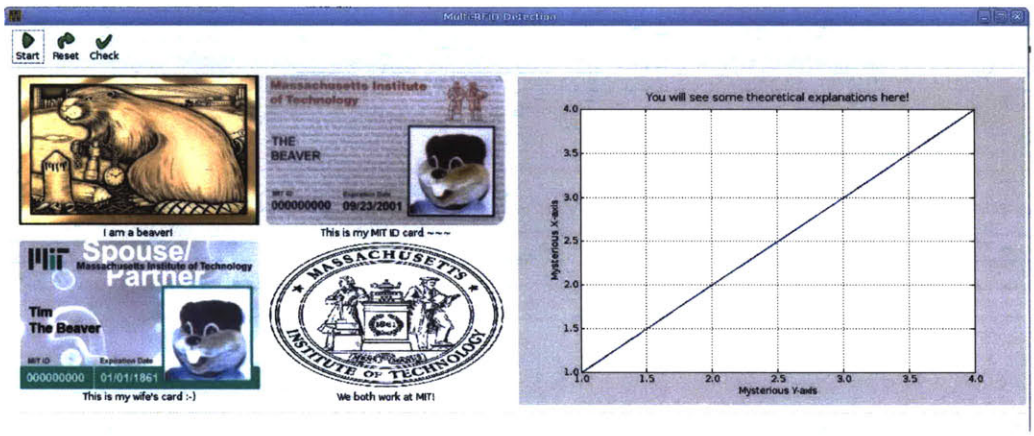

Figure 3-13 – The graphical user interface of the multiple RFID cards' reader, built using PyGTK

perform symbol synchronization to find the right timing to down-sample the signal.

3.3.6 Putting Everything Together

Integrating all modules discussed above together, we build a complete, operational multiple RFID card reader. A complete system design diagram is shown in Figure.3-12.

The reader was demonstrated in the MIT Media Lab's sponsor meeting held in May, 2007. It was capable of reading four cards. A graphical interface is shown in Figure.3-13.

3.4 Summary

In this section, we introduce a complete design of a multiple RFID cards' reader using GNU Software Radio. In addition to the algorithm development, design choices, practical issues in both software and hardware are discussed and explored.

The multiple RFID card reader is a strong demonstration of the digital signal separation concept. The message delivered from such a system is: judiciously building the receiver using more advanced digital signal processing techniques allows simultaneous transmissions, thus improving the throughput of the network system and bringing great convenience and experience to the users.

We finish up this chapter by pointing out that such a multiple RFID card reader can be further improved by considering time diversity. Because each card transmits the same 224 bits repeatedly and continuously, we can actually do soft combining (or diversity combining) to enhance the decoding performance considerably. This will be explored in future research.

Chapter 4

Optimum Frame Synchronization

In Chapter 4, we study the problem of frame synchronization for multiple access channels (MAC). We propose several decision rules for locating the starting sample of a transmitted frame. We show that the commonly utilized correlation rule is only suboptimal and that a correction term needs to be considered to achieve the best detection performance. The main focus of this chapter is on the frame-asynchronous case. We show that the joint estimation rule is optimal in theory, but it leads to an intractable decision rule. A much simpler algorithm using Gaussian approximation reduces the computational complexity significantly, while sacrificing only a small amount of optimality.

4.1 Introduction

In current communication systems, frame synchronization is achieved by inserting a fixed symbol pattern or 'sync word' periodically into the data stream, assuming symbol-level synchronization has already been obtained. The receiver needs to locate the position of the sync word in the received data stream. In his pioneer work, Massey derived the optimal decision rule and demonstrated that the optimal rule was to select the location that maximized the sum of the correlation and a correction term [15].

This rule outperformed the commonly used correlation rule.

Researchers have made a few extensions from Massey's work. However, most of these were developed for point-to-point channels. Little attention has been paid to multiple-input multiple output(MIMO) channels and multiple access chanels (MAC). In the RFID signal separation problem, all signals are transmitted continuously and repeatedly, with fixed sync words inserted into the data streams (30 zeros, or the 192 constant bits). Meanwhile, all signals are synchronous at the symbol level. This particular system perfectly fits into the research domain of frame synchronization, which motivates us to explore the optimal decision criteria for multiple-input single-output channels, which we also usually call multiple access channels (MAC).

Because of its theoretical importance, we devote the whole chapter 4 to this topic. The optimal decision rules developed in this chapter will be very useful in separating digital signals that are linearly modulated such as MPSK or QAM.

4.2 The General MIMO Channel

Let's consider the MIMO channel first. Though we use a single antenna in the multiple RFID cards' reader, it's helpful to study the more general MIMO channel model first to obtain some insights. The results will be directly applicable if we use multiple antennas in our future system design. We consider the MIMO channel model

$$\boldsymbol{y} = \boldsymbol{H}\boldsymbol{x} + \boldsymbol{n}. \tag{4.1}$$

In the RFID system, all computation is performed with real-valued samples. To make our analysis more general, we assume all entries here are complex-valued. $\boldsymbol{H}$ is a $m \times n$ complex matrix whose random coefficients are independent of $\boldsymbol{x}$ and $\boldsymbol{n}$. The realization of $\boldsymbol{H}$ is perfectly known at the receiver as H, and the transmitter has no knowledge of $\boldsymbol{H}$. $\boldsymbol{n}$ is zero-mean complex additive white Gaussian noise with $E[\boldsymbol{n}\boldsymbol{n}^{\dagger}] = \mathrm{N}I_m$.

We consider the case when n transmitters have the same frame length N. Each transmitter l has its own sync word $(s_{l,0}, s_{l,1}, \ldots, s_{l,L-1})$. Here we assume n transmitters are synchronized such that they transmit the sync words at the same time. This is not a valid assumption for the multiple RFID cards' system, but it is valid in a pre-coordinated system. We will get back to the frame-asynchronous case for MAC channels later. In the next chapter, we will discuss a protocol that achieves synchronization among multiple transmitters. All transmitted symbols within a frame are denoted using the elements in a matrix $\boldsymbol{T}$,

$$\boldsymbol{T}_{n\times N} = \begin{pmatrix} s_{1,0} & s_{1,1} & \cdots & s_{1,L-1} & \boldsymbol{d}_{1,L} & \boldsymbol{d}_{1,L+1} & \cdots & \boldsymbol{d}_{1,N-1} \\ s_{2,0} & s_{2,1} & \cdots & s_{2,L-1} & \boldsymbol{d}_{2,L} & \boldsymbol{d}_{2,L+1} & \cdots & \boldsymbol{d}_{2,N-1} \\ \vdots & \vdots & \ddots & \vdots & \vdots & \vdots & \ddots & \vdots \\ s_{n,0} & s_{n,1} & \cdots & s_{n,L-1} & \boldsymbol{d}_{n,L} & \boldsymbol{d}_{n,L+1} & \cdots & \boldsymbol{d}_{n,N-1} \end{pmatrix}. \tag{4.2}$$

The l^{th} row of $\boldsymbol{T}$ is the frame transmitted by the antenna l. The sub-matrix $\boldsymbol{D}$, with elements $\boldsymbol{d}_{i,j}(1 \leq i \leq n, L \leq j \leq N-1)$, denotes the payload data symbols where $\boldsymbol{d}_{i,j}$ are statistically independent. The sub-matrix S, with elements $s_{i,j}(1 \leq i \leq n, 0 \leq j \leq L-1)$, denotes the sync codewords matrix. $\boldsymbol{D}$ is unknown at the receivers but the sync codewords matrix S is. Each element $s_{i,j}$ or $\boldsymbol{d}_{i,j}$ represents for a transmitted symbol, which corresponds to a point in a 2-dimensional M-constellation. For example, the constellation can be MPSK or QAM, where all M points, denoted as $(w_1, w_2, \ldots, w_M)$, are equally probable with a probability of $1/M$.

The received m frames at the m receiving antennas in the noiseless frame-synchronous case is thus

$$\boldsymbol{Q}_{m\times N} = H_{m\times n}\boldsymbol{T}_{n\times N} = \begin{pmatrix} t_{1,0} & t_{1,1} & \cdots & t_{1,L-1} & \boldsymbol{c}_{1,L} & \boldsymbol{c}_{1,L+1} & \cdots & \boldsymbol{c}_{1,N-1} \\ t_{2,0} & t_{2,1} & \cdots & t_{2,L-1} & \boldsymbol{c}_{2,L} & \boldsymbol{c}_{2,L+1} & \cdots & \boldsymbol{c}_{2,N-1} \\ \vdots & \vdots & \ddots & \vdots & \vdots & \vdots & \ddots & \vdots \\ t_{m,0} & t_{m,1} & \cdots & t_{m,L-1} & \boldsymbol{c}_{m,L} & \boldsymbol{c}_{m,L+1} & \cdots & \boldsymbol{c}_{m,N-1} \end{pmatrix}, \tag{4.3}$$

where

$$t_{k,i} = \sum_{l=1}^{n} h_{k,l} s_{l,i}, \quad 1 \le k \le m, 0 \le i \le L-1, \tag{4.4}$$

$$\boldsymbol{c}_{k,j} = \sum_{l=1}^{n} h_{k,l} \boldsymbol{d}_{l,j}, \quad 1 \le k \le m, L \le j \le N-1. \tag{4.5}$$

We emphasize again that $t_{k,i}$ are known by the receiver while the sub-matrix $\boldsymbol{C}$ is random.

The actual received frames can be expressed as

$$\boldsymbol{R}_{m\times N} = \mathrm{T}^{\boldsymbol{\mu}}(\boldsymbol{Q}_{m\times N}) + \boldsymbol{N}_{m\times N}, \tag{4.6}$$

where T^{μ} is the cyclic right shift operator. We use R, the observation of $\boldsymbol{R}$, to estimate the optimal sync word position $\boldsymbol{\mu}$. The optimum decision rule (MAP) is to choose the estimate of $\boldsymbol{\mu}$ as the value $\mu (0 \le \mu \le N-1)$, which maximizes $S_1 = \Pr[\boldsymbol{\mu} = \mu | \boldsymbol{R} = R] = p_{\boldsymbol{R}}(R|\boldsymbol{\mu} = \mu) \Pr[\boldsymbol{\mu} = \mu] / p_{\boldsymbol{R}}(R)$. Since $\Pr[\boldsymbol{\mu} = \mu] = 1/N$ for all μ, we may equivalently maximize $S_2 = p_{\boldsymbol{R}}(R|\boldsymbol{\mu} = \mu)$. Equivalently, we could maximize

$$S_2 = \sum_{\text{all}D} p_{\boldsymbol{R}}(R|\boldsymbol{D} = D, \boldsymbol{\mu} = \mu) \Pr[\boldsymbol{D} = D]. \tag{4.7}$$

Since $\Pr[\boldsymbol{D} = D] = \left(\frac{1}{M}\right)^{n(N-L)}$ for all D, we may equivalently maximize

$$S_3 = \sum_{\text{all}D} p_{\boldsymbol{R}}(R|\boldsymbol{D} = D, \boldsymbol{\mu} = \mu),$$

which upon making use of (4.6) becomes

$$S_3 = \sum_{\text{all}D} p_{\boldsymbol{N}}(R - \mathrm{T}^{\mu}(Q)). \tag{4.8}$$

$\boldsymbol{N}$ is complex Gaussian distributed. Thus, we have

$$p_{\boldsymbol{N}}(R - \mathrm{T}^{\mu}(Q)) = (\pi\mathbf{N})^{-mN} \left[\prod_{i=0}^{L-1}\prod_{k=1}^{m} e^{-|r_{k,i+\mu}-t_{k,i}|^2/\mathbf{N}}\right] \left[\prod_{j=L}^{N-1}\prod_{k=1}^{m} e^{-|r_{k,j+\mu}-c_{k,j}|^2/\mathbf{N}}\right].$$

Substituting $p_{\boldsymbol{N}}(R - \mathrm{T}^{\mu}(Q))$ into (4.8) and removing all terms independent of μ, we can equivalently maximize

$$\begin{aligned} S_4 &= \sum_{\text{all}D} \left[\prod_{i=0}^{L-1}\prod_{k=1}^{m} e^{(r_{k,i+\mu}t^*_{k,i}+r^*_{k,i+\mu}t_{k,i})/\mathbf{N}}\right] \left[\prod_{j=L}^{N-1}\prod_{k=1}^{m} e^{(r_{k,j+\mu}c^*_{k,j}+r^*_{k,j+\mu}c_{k,j}-|c_{k,j}|^2)/\mathbf{N}}\right] \\ &= \left[\prod_{i=0}^{L-1}\prod_{k=1}^{m}\prod_{l=1}^{n} e^{(r_{k,i+\mu}h^*_{k,l}s^*_{l,i}+r^*_{k,i+\mu}h_{k,l}s_{l,i})/\mathbf{N}}\right] \\ &\quad \cdot \sum_{\text{all}D} \left[\prod_{j=L}^{N-1}\prod_{k=1}^{m} e^{(\sum_{l=1}^{n}(r_{k,j+\mu}h^*_{k,l}d^*_{l,j}+r^*_{k,j+\mu}h_{k,l}d_{l,j})-|\sum_{l=1}^{n}h_{k,l}d_{l,j}|^2)/\mathbf{N}}\right]. \end{aligned} \tag{4.9}$$

Let $\underline{\boldsymbol{d}}_j (L \le j \le N-1)$ denote $(d_{1,j}, d_{2,j}, \cdots, d_{n,j})^T$, the jth column of the submatrix $\boldsymbol{D}$. Note that since each $d_{l,j}$ takes on values from M equally probable points $(w_1, w_2, \ldots, w_M)$, $\underline{\boldsymbol{d}}_j$ is uniformly distributed among M^n possible vectors $(\underline{v}_1, \underline{v}_2, \ldots, \underline{v}_{M^n})$, which are different combinations of w_l's. Then, we obtain

$$\begin{aligned} S_4 &= \left[\prod_{i=0}^{L-1}\prod_{k=1}^{m}\prod_{l=1}^{n} e^{(r_{k,i+\mu}h^*_{k,l}s^*_{l,i}+r^*_{k,i+\mu}h_{k,l}s_{l,i})/\mathbf{N}}\right] \\ &\quad \cdot \left[\prod_{j=L}^{N-1}\prod_{k=1}^{m} \left(\sum_{\underline{v}=\underline{v}_1}^{\underline{v}_{M^n}} e^{(\sum_{l=1}^{n}(r_{k,j+\mu}h^*_{k,l}v^*_l+r^*_{k,j+\mu}h_{k,l}v_l)-|\sum_{l=1}^{n}h_{k,l}v_l|^2)/\mathbf{N}}\right)\right], \end{aligned} \tag{4.10}$$

where v_l is the lth element of the vector $\underline{v}$. Taking natural logarithms, we can equivalently maximize

$$\begin{aligned} S_5 &= \sum_{i=0}^{L-1}\sum_{k=1}^{m}\sum_{l=1}^{n}(r_{k,i+\mu}h^*_{k,l}s^*_{l,i} + r^*_{k,i+\mu}h_{k,l}s_{l,i})/\mathbf{N} \\ &\quad + \sum_{j=L}^{N-1}\sum_{k=1}^{m} \left[\ln\left(\sum_{\underline{v}=\underline{v}_1}^{\underline{v}_{M^n}} e^{(\sum_{l=1}^{n}(r_{k,j+\mu}h^*_{k,l}v^*_l+r^*_{k,j+\mu}h_{k,l}v_l)-|\sum_{l=1}^{n}h_{k,l}v_l|^2)/\mathbf{N}}\right)\right] \end{aligned} \tag{4.11}$$

Also, noting that

$$\sum_{j=0}^{N-1}\sum_{k=1}^{m}\left[\ln\left(\sum_{\underline{v}=\underline{v}_1}^{\underline{v}_{M^n}} e^{(\sum_{l=1}^{n}(r_{k,j+\mu}h_{k,l}^{*}v_l^{*}+r_{k,j+\mu}^{*}h_{k,l}v_l)-|\sum_{l=1}^{n}h_{k,l}v_l|^2)/\mathbf{N}}\right)\right]$$

is independent of μ, we may subtract this sum from S_5 and give

$$\begin{aligned} S_6 &= \frac{1}{\mathbf{N}}\sum_{i=0}^{L-1}\sum_{k=1}^{m}\sum_{l=1}^{n}(r_{k,i+\mu}h_{k,l}^{*}s_{l,i}^{*}+r_{k,i+\mu}^{*}h_{k,l}s_{l,i}) \\ &\quad -\sum_{i=0}^{L-1}\sum_{k=1}^{m}\left[\ln\left(\sum_{\underline{v}=\underline{v}_1}^{\underline{v}_{M^n}} e^{(\sum_{l=1}^{n}(r_{k,i+\mu}h_{k,l}^{*}v_l^{*}+r_{k,i+\mu}^{*}h_{k,l}v_l)-|\sum_{l=1}^{n}h_{k,l}v_l|^2)/\mathbf{N}}\right)\right] \end{aligned} \quad (4.12)$$

The sum S_6 can be represented using the matrix form. Let the matrix

$$A_{N\times L}=R_{N\times m}^{\mathrm{T}}H_{m\times n}^{*}S_{n\times L}^{*} \qquad A_{N\times L}^{*}=R_{N\times m}^{\dagger}H_{m\times n}S_{n\times L},$$

where $a_{i,j}=\sum_{k=1}^{m}\sum_{l=1}^{n}r_{k,i}h_{k,l}^{*}s_{l,j}^{*}$. Then, S_6 can be represented as

$$\begin{aligned} S_6 &= \frac{1}{\mathbf{N}}\sum_{i=0}^{L-1}(a_{i+\mu,i}+a_{i+\mu,i}^{*}) \\ &\quad -\sum_{i=0}^{L-1}\sum_{k=1}^{m}\left[\ln\left(\sum_{\underline{v}=\underline{v}_1}^{\underline{v}_{M^n}} e^{(\sum_{l=1}^{n}(r_{k,i+\mu}h_{k,l}^{*}v_l^{*}+r_{k,i+\mu}^{*}h_{k,l}v_l)-|\sum_{l=1}^{n}h_{k,l}v_l|^2)/\mathbf{N}}\right)\right] \end{aligned} \quad (4.13)$$

Again, this is a correlation term adjusted by a correction term.

4.3 The Multiple Access Channel

The channel model for the multiple RFID cards' system is actually a simplified version of the multiple access channel(MAC) model. We consider the multiple access channel model

$$\boldsymbol{y}=\underline{\boldsymbol{h}}^{\mathrm{T}}\underline{\boldsymbol{x}}+\boldsymbol{z}=\sum_{l=1}^{n}\boldsymbol{h}_l\boldsymbol{x}_l+\boldsymbol{z}. \quad (4.14)$$

$\underline{\boldsymbol{h}}$ is a length-n complex vector whose random coefficients are independent of $\underline{\boldsymbol{x}}$ and $\boldsymbol{z}$. The realization of $\underline{\boldsymbol{h}}$ is perfectly known at the receiver as $\underline{h}$, and the transmitter has no knowledge of $\underline{\boldsymbol{h}}$. The scalar $\boldsymbol{z}$ is the zero-mean complex additive white Gaussian noise with the variance σ^2.

4.3.1 The Frame-Synchronous Case

If all n transmitters transmit frames in a synchronous manner, the MAC model can be viewed as a simplified case of the MIMO channel model with $m = 1$. The received frame in a noiseless environment is

$$\underline{\boldsymbol{q}}_{1\times N} = \underline{h}^{\mathrm{T}}_{1\times n}\boldsymbol{T}_{n\times N} = (t_0, t_1, \cdots, t_{L-1}, \boldsymbol{c}_L, \boldsymbol{c}_{L+1}, \cdots, \boldsymbol{c}_{N-1}), \tag{4.15}$$

where

$$t_i = \sum_{l=1}^{n} h_l s_{l,i} \quad (0 \le i \le L-1), \quad \boldsymbol{c}_j = \sum_{l=1}^{n} h_l \boldsymbol{d}_{l,j} \quad (L \le j \le N-1). \tag{4.16}$$

The actual received frame considering the noise and the shift can be expressed as

$$\underline{\boldsymbol{r}}_{1\times N} = \mathrm{T}^{\boldsymbol{\mu}}(\underline{\boldsymbol{q}}_{1\times N}) + \underline{\boldsymbol{z}}_{1\times N}, \tag{4.17}$$

Following the steps derived for the MIMO channel, we obtain the MAP rule for estimating $\boldsymbol{\mu}$ is to choose a value μ that maximizes

$$S_{3,\mathrm{MAC}} = \sum_{\mathrm{all}D} p_{\underline{\boldsymbol{z}}}(\underline{r} - \mathrm{T}^{\mu}(\underline{q})). \tag{4.18}$$

$\underline{\boldsymbol{z}}$ is complex Gaussian distributed. Thus, we have

$$p_{\underline{\boldsymbol{z}}}(\underline{r} - \mathrm{T}^{\mu}(\underline{q})) = (\pi\sigma^2)^{-N} \left[\prod_{i=0}^{L-1} e^{-|r_{i+\mu} - t_i|^2/\sigma^2}\right] \left[\prod_{j=L}^{N-1} e^{-|r_{j+\mu} - c_j|^2/\sigma^2}\right].$$

Substitude $p_{\underline{z}}(\underline{r} - \mathrm{T}^{\mu}(\underline{q}))$ into (4.18) and removing all terms independent of μ, we can equivalently maximize

$$\begin{aligned} S_{4,\mathrm{MAC}} &= \sum_{\mathrm{all}D} \left[\prod_{i=0}^{L-1} e^{(r_{i+\mu}t_i^* + r_{i+\mu}^* t_i)/\sigma^2} \right] \left[\prod_{j=L}^{N-1} e^{(r_{j+\mu}c_j^* + r_{j+\mu}^* c_j - |c_j|^2)/\sigma^2} \right] \\ &= \left[\prod_{i=0}^{L-1} \prod_{l=1}^{n} e^{(r_{i+\mu}h_l^* s_{l,i}^* + r_{i+\mu}^* h_l s_{l,i})/\sigma^2} \right] \\ &\quad \cdot \left[\prod_{j=L}^{N-1} \left(\sum_{\underline{v}=\underline{v}_1}^{\underline{v}_{M^n}} e^{(\sum_{l=1}^{n}(r_{j+\mu}h_l^* v_l^* + r_{j+\mu}^* h_l v_l) - |\sum_{l=1}^{n} h_l v_l|^2)/\sigma^2} \right) \right], \end{aligned} \tag{4.19}$$

where the meanings of $\underline{v}$'s are the same as those in the MIMO case. By taking the logarithm and removing a term independent of μ, we obtain

$$\begin{aligned} S_{6,\mathrm{MAC}} &= \frac{1}{\sigma^2} \sum_{i=0}^{L-1} \sum_{l=1}^{n} (r_{i+\mu}h_l^* s_{l,i}^* + r_{i+\mu}^* h_l s_{l,i}) \\ &\quad - \sum_{i=0}^{L-1} \left[\ln \left(\sum_{\underline{v}=\underline{v}_1}^{\underline{v}_{M^n}} e^{(\sum_{l=1}^{n}(r_{i+\mu}h_l^* v_l^* + r_{i+\mu}^* h_l v_l) - |\sum_{l=1}^{n} h_l v_l|^2)/\sigma^2} \right) \right]. \end{aligned} \tag{4.20}$$

The Monte Carlo simulation results are shown in Figure.4-1, 4-2 and 4-3. We assume two transmitters are frame-synchronized and they send BPSK signals. They both use a 13-bit Barker code as the sync-word. The length of a frame is set to 91, as Massey did in his work. The amplitude of the first sender h_1 is fixed as 1, and h_2 is chosen as 0.8, 0.5 and 0.2 respectively in Figure.4-1, 4-2 and 4-3. The noise variance σ^2 ranges from 0.5 to 9.5, which typically represents the low SNR case. We can observe that the optimal decision rule outperforms the traditional correlation rule distinctly. The benefit of applying the optimal decision rule is most evident when σ^2 ranges from 2 to 6. When σ^2 is less than 2, both the optimal rule and the correlation rule can do almost equally well in the high SNR scenario. When the noise level is too high, both methods produce errors frequently. As h_2 decreases, the detection performance of both rules degrades, because the energy in the correlation term becomes smaller.

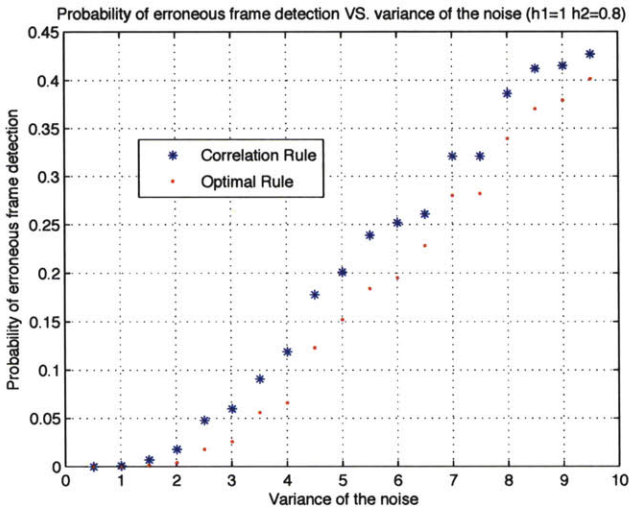

Figure 4-1 – The comparison between the correlation rule and the optimal decision rule for frame detection in the frame-synchronous case. Two transmitters use Barker codes, $h_1 = 1$, $h_2 = 0.8$, noise variance (σ^2) ranges from 0.5 to 9.5

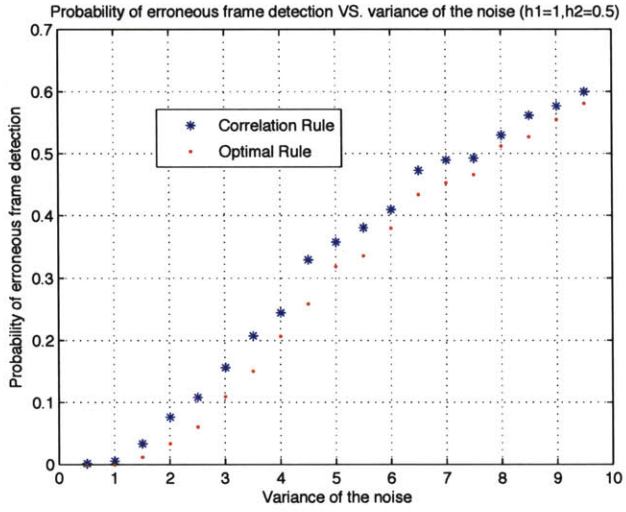

Figure 4-2 – The comparison between the correlation rule and the optimal decision rule for frame detection in the frame-synchronous case. Two transmitters use Barker codes, $h_1 = 1$, $h_2 = 0.5$, noise variance (σ^2) ranges from 0.5 to 9.5

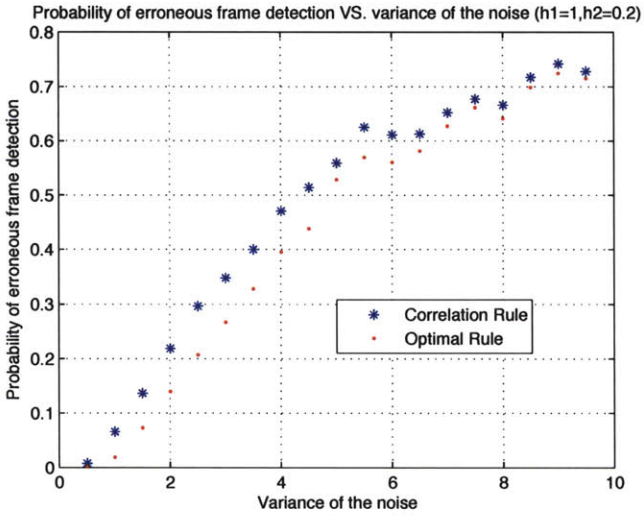

Figure 4-3 – The comparison between the correlation rule and the optimal decision rule for frame detection in the frame-synchronous case. Two transmitters use Barker codes, $h_1 = 1$, $h_2 = 0.2$, noise variance (σ^2) ranges from 0.5 to 9.5

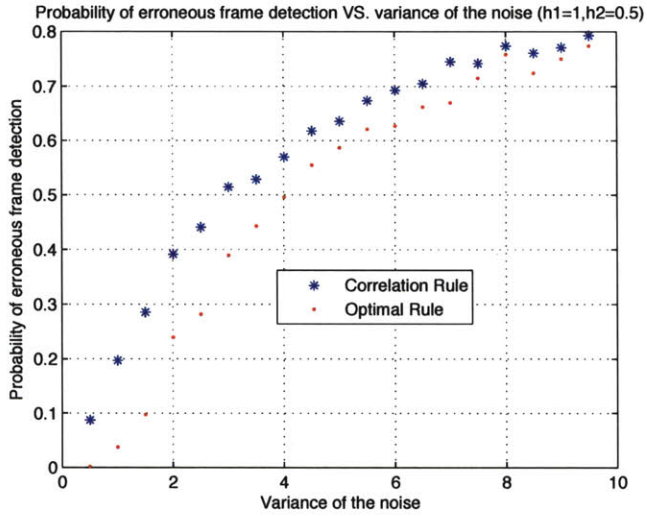

Figure 4-4 – The comparison between the correlation rule and the optimal decision rule for frame detection in the frame-synchronous case. Two transmitters use random sync-words, $h_1 = 1$, $h_2 = 0.5$, noise variance (σ^2) ranges from 0.5 to 9.5

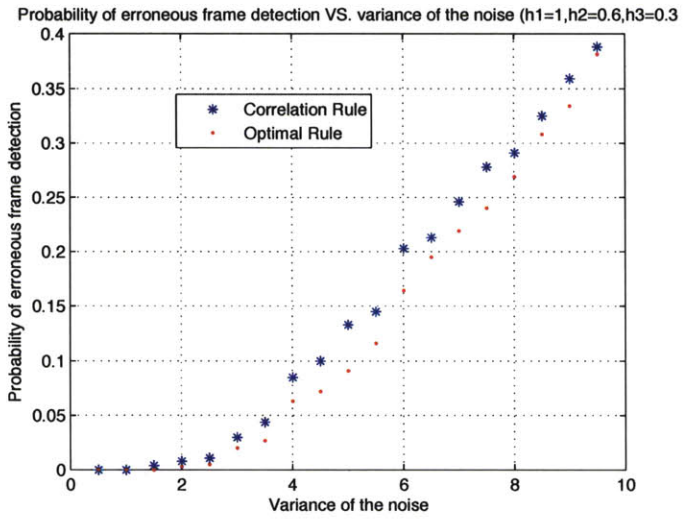

Figure 4-5 – The comparison between the correlation rule and the optimal decision rule for frame detection in the frame-synchronous case. Three transmitters use Barker codes, $h_1 = 1$, $h_2 = 0.6$,$h_3 = 0.3$, noise variance (σ^2) ranges from 0.5 to 9.5

In the previous simulation results, we use the same Barker code as the sync-word for both transmitters. Barker code is widely used for its low-autocorrelation property. In Figure.4-4, we show the simulation results when we use randomly-generated sync-words for both transmitters. h_1 and h_2 are set to 1 and 0.5. In each run, we randomly generate two different sync-words for the two transmitters and make them available to the receiver. Compared with Figure.4-2, Figure.4-4 shows that a Barker code performs better than a randomly chosen sync-word.

Figure.4-5 shows the 3-transmitter case when $h_1 = 1$, $h_2 = 0.6$, $h_3 = 0.3$. As anticipated, the optimal decision rule works more accurately than the correlation rule. Also, the error rate of frame detection is lower when compared with the 2-transmitter case because the energy in the correlation term gets larger.

4.3.2 The Frame-Asynchronous Case

Now we consider the case when n transmitters start transmitting frames at different time instants. We assume the transmitters are synchronous at the sym-

bol level. Instead of estimating one sync word position $\boldsymbol{\mu}$, we need to estimate n sync word positions for all transmitters, which we represent using a random vector $\underline{\boldsymbol{\mu}} = (\boldsymbol{\mu}_1, \boldsymbol{\mu}_2, \cdots, \boldsymbol{\mu}_n)^{\mathrm{T}}$.

There are two approaches of estimating $\underline{\boldsymbol{\mu}}$. First, we can estimate $\boldsymbol{\mu}_k (1 \leq k \leq n)$ separately for each transmitter. In this case, we assume all the other $n-1$ transmitters constantly transmit random data symbols spanning the whole length-N frame. The knowledge of the known sync words contained in the symbols is simply ignored. Secondly, we can jointly estimate all $\boldsymbol{\mu}_k$'s $(1 \leq k \leq n)$ using the MAP rule. Obviously, the second method is optimal, but it requires a more complicated algorithm.

The Separate Estimation Approach

Without loss of generality, we assume that we need to estimate the sync word position $\boldsymbol{\mu}$ for the transmitter 1. The transmitted symbols in a frame of the n transmitters are denoted using a matrix $\boldsymbol{T}^s$,

$$\boldsymbol{T}^s_{n\times N} = \begin{pmatrix} s_0 & s_1 & \cdots & s_{L-1} & \boldsymbol{d}_{1,L} & \boldsymbol{d}_{1,L+1} & \cdots & \boldsymbol{d}_{1,N-1} \\ \boldsymbol{d}_{2,0} & \boldsymbol{d}_{2,1} & \cdots & \boldsymbol{d}_{2,L-1} & \boldsymbol{d}_{2,L} & \boldsymbol{d}_{2,L+1} & \cdots & \boldsymbol{d}_{2,N-1} \\ \vdots & \vdots & \ddots & \vdots & \vdots & \vdots & \ddots & \vdots \\ \boldsymbol{d}_{n,0} & \boldsymbol{d}_{n,1} & \cdots & \boldsymbol{d}_{n,L-1} & \boldsymbol{d}_{n,L} & \boldsymbol{d}_{n,L+1} & \cdots & \boldsymbol{d}_{n,N-1} \end{pmatrix}. \tag{4.21}$$

Compared with $\boldsymbol{T}$ in (4.2), the symbols under the sync word $(s_0, s_1, \cdots, s_{L-1})$ are no longer known sync words, but unknown random symbols. The submatrix under the sync word, containing elements $\boldsymbol{d}_{l,i} (2 \leq l \leq n, 0 \leq i \leq L-1)$ is denoted as $\boldsymbol{D'}$. The received frame excluding the noise can be calculated as

$$\underline{\boldsymbol{q}}^s_{1\times N} = \underline{h}^{\mathrm{T}}_{1\times n} \boldsymbol{T}^s_{n\times N} = (\boldsymbol{t}_0, \boldsymbol{t}_1, \cdots, \boldsymbol{t}_{L-1}, \boldsymbol{c}_L, \boldsymbol{c}_{L+1}, \cdots, \boldsymbol{c}_{N-1}), \tag{4.22}$$

where

$$\boldsymbol{t}_i = h_1 s_i + \sum_{l=2}^{n} h_l \boldsymbol{d}_{l,i}, \quad 0 \leq i \leq L-1, \tag{4.23}$$

$$\boldsymbol{c}_j = \sum_{l=1}^{n} h_l \boldsymbol{d}_{l,j}, \quad L \leq j \leq N-1. \tag{4.24}$$

Note that here we use a superscript 's' to indicate this equation is derived for 'separate estimation'. Taking the unknown shift $\boldsymbol{\mu}$ and the additive white Gaussian noise into consideration, the actual received frame at the receiver is

$$\underline{\boldsymbol{r}}^s_{1\times N} = \mathrm{T}^{\boldsymbol{\mu}}(\underline{\boldsymbol{q}}^s_{1\times N}) + \underline{\boldsymbol{z}}_{1\times N}, \tag{4.25}$$

Following the derivations for the MIMO case, the MAP rule for estimating $\boldsymbol{\mu}$ leads us to maximize

$$S_2^s = \sum_{\text{all}D} \sum_{\text{all}D'} p_{\underline{\boldsymbol{r}}^s}(\underline{r}^s | \boldsymbol{D} = D, \boldsymbol{D'} = D', \boldsymbol{\mu} = \mu) \Pr[\boldsymbol{D} = D, \boldsymbol{D'} = D']. \tag{4.26}$$

Since $\Pr[\boldsymbol{D} = D, \boldsymbol{D'} = D'] = \left(\frac{1}{M}\right)^{(nN-L)}$ for all D, D', we may equivalently maximize

$$S_3^s = \sum_{\text{all}D} \sum_{\text{all}D'} p_{\underline{\boldsymbol{r}}^s}(\underline{r}^s | \boldsymbol{D} = D, \boldsymbol{D'} = D', \boldsymbol{\mu} = \mu),$$

which upon making use of (4.25) becomes

$$S_3^s = \sum_{\text{all}D} \sum_{\text{all}D'} p_{\underline{\boldsymbol{z}}}(\underline{r}^s - \mathrm{T}^{\mu}(\underline{q}^s)). \tag{4.27}$$

$\underline{\boldsymbol{z}}$ is complex Gaussian distributed. Thus, we have

$$p_{\underline{\boldsymbol{z}}}(\underline{r}^s - \mathrm{T}^{\mu}(\underline{q}^s)) = (\pi\sigma^2)^{-N} \left[\prod_{i=0}^{L-1} e^{-|r_{i+\mu} - t_i|^2/\sigma^2}\right] \left[\prod_{j=L}^{N-1} e^{-|r_{j+\mu} - c_j|^2/\sigma^2}\right].$$

Substituting $p_{\underline{z}}(\underline{r}^s - \mathrm{T}^{\mu}(\underline{q}^s))$ into (4.27) and removing all terms independent of μ, we can equivalently maximize

$$\begin{aligned} S_4^s &= \sum_{\text{all}D} \sum_{\text{all}D'} \left[\prod_{i=0}^{L-1} e^{(r_{i+\mu} t_i^* + r_{i+\mu}^* t_i - |t_i|^2)/\sigma^2} \right] \left[\prod_{j=L}^{N-1} e^{(r_{j+\mu} c_j^* + r_{j+\mu}^* c_j - |c_j|^2)/\sigma^2} \right] \\ &= \sum_{\text{all}D'} \left[\prod_{i=0}^{L-1} e^{((r_{i+\mu} h_1^* s_i^* + r_{i+\mu}^* h_1 s_i) + \sum_{l=2}^{n} (r_{i+\mu} h_l^* d_{l,i}^* + r_{i+\mu}^* h_l d_{l,i}) - |h_1 s_i + \sum_{l=2}^{n} h_l d_{l,i}|^2)/\sigma^2} \right] \\ &\quad \cdot \sum_{\text{all}D} \left[\prod_{j=L}^{N-1} e^{(\sum_{l=1}^{n} (r_{j+\mu} h_l^* d_{l,j}^* + r_{j+\mu}^* h_l d_{l,j}) - |\sum_{l=1}^{n} h_l d_{l,j}|^2)/\sigma^2} \right]. \end{aligned} \tag{4.28}$$

Let $\underline{\boldsymbol{d}}_j (L \leq j \leq N-1)$ denote $(d_{1,j}, d_{2,j}, \cdots, d_{n,j})^T$, the jth column of the sub-matrix $\boldsymbol{D}$, $\underline{\boldsymbol{d}}'_i (0 \leq i \leq L-1)$ denote $(d_{2,i}, d_{3,i}, \cdots, d_{n,i})^T$, the ith column of the sub-matrix $\boldsymbol{D'}$. Note that since each $d_{l,j}$ takes on values from M equally probable points $(w_1, w_2, \ldots, w_M)$, $\underline{\boldsymbol{d}}_j$ is uniformly distributed among M^n possible vectors $(\underline{v}_1, \underline{v}_2, \ldots, \underline{v}_{M^n})$, $\underline{\boldsymbol{d}}'_i$ is uniformly distributed among $M^{(n-1)}$ possible vectors $(\underline{u}_1, \underline{u}_2, \ldots, \underline{u}_{M^{(n-1)}})$, which are different combinations of w_l's. Then, we obtain

$$\begin{aligned} S_4^s &= \left[\prod_{i=0}^{L-1} e^{(r_{i+\mu} h_1^* s_i^* + r_{i+\mu}^* h_1 s_i)/\sigma^2} \left(\sum_{\underline{u}=\underline{u}_1}^{\underline{u}_{M^{n-1}}} e^{(\sum_{l=2}^{n} (r_{i+\mu} h_l^* u_l^* + r_{i+\mu}^* h_l u_l) - |h_1 s_i + \sum_{l=2}^{n} h_l u_l|^2)/\sigma^2} \right) \right] \\ &\quad \cdot \left[\prod_{j=L}^{N-1} \left(\sum_{\underline{v}=\underline{v}_1}^{\underline{v}_{M^n}} e^{(\sum_{l=1}^{n} (r_{j+\mu} h_l^* v_l^* + r_{j+\mu}^* h_l v_l) - |\sum_{l=1}^{n} h_l v_l|^2)/\sigma^2} \right) \right], \end{aligned} \tag{4.29}$$

where v_l is the lth element of the vector $\underline{v}$ and where u_l is the $(l-1)$th element of the vector $\underline{u}$. Taking natural logarithms, we can equivalently maximize

$$\begin{aligned} S_5^s &= \frac{1}{\sigma^2}\sum_{i=0}^{L-1}(r_{i+\mu}h_1^*s_i^* + r_{i+\mu}^*h_1s_i) \\ &\quad + \sum_{i=0}^{L-1}\left[\ln\left(\sum_{\underline{u}=\underline{u}_1}^{\underline{u}_{M^{n-1}}} e^{(\sum_{l=2}^{n}(r_{i+\mu}h_l^*u_l^* + r_{i+\mu}^*h_lu_l) - |h_1s_i + \sum_{l=2}^{n}h_lu_l|^2)/\sigma^2}\right)\right] \\ &\quad + \sum_{j=L}^{N-1}\left[\ln\left(\sum_{\underline{v}=\underline{v}_1}^{\underline{v}_{M^n}} e^{(\sum_{l=1}^{n}(r_{j+\mu}h_l^*v_l^* + r_{j+\mu}^*h_lv_l) - |\sum_{l=1}^{n}h_lv_l|^2)/\sigma^2}\right)\right], \end{aligned} \tag{4.30}$$

Also, noting that

$$\sum_{j=0}^{N-1}\left[\ln\left(\sum_{\underline{v}=\underline{v}_1}^{\underline{v}_{M^n}} e^{(\sum_{l=1}^{n}(r_{j+\mu}h_l^*v_l^* + r_{j+\mu}^*h_lv_l) - |\sum_{l=1}^{n}h_lv_l|^2)/\sigma^2}\right)\right]$$

is independent of μ, we may subtract it from S_5^s and give

$$\begin{aligned} S_6^s &= \frac{1}{\sigma^2}\sum_{i=0}^{L-1}(r_{i+\mu}h_1^*s_i^* + r_{i+\mu}^*h_1s_i) \\ &\quad + \sum_{i=0}^{L-1}\left[\ln\left(\sum_{\underline{u}=\underline{u}_1}^{\underline{u}_{M^{n-1}}} e^{(\sum_{l=2}^{n}(r_{i+\mu}h_l^*u_l^* + r_{i+\mu}^*h_lu_l) - |h_1s_i + \sum_{l=2}^{n}h_lu_l|^2)/\sigma^2}\right)\right] \\ &\quad - \sum_{i=0}^{L-1}\left[\ln\left(\sum_{\underline{v}=\underline{v}_1}^{\underline{v}_{M^n}} e^{(\sum_{l=1}^{n}(r_{i+\mu}h_l^*v_l^* + r_{i+\mu}^*h_lv_l) - |\sum_{l=1}^{n}h_lv_l|^2)/\sigma^2}\right)\right], \end{aligned} \tag{4.31}$$

Selecting a μ to maximize S_6^s is the optimal decision rule for separately estimating the frame starting position $\boldsymbol{\mu}$ for one single transmitter. The term $\frac{1}{\sigma^2}\sum_{i=0}^{L-1}(r_{i+\mu}h_1^*s_i^* + r_{i+\mu}^*h_1s_i)$ is the correlation between the sync word and the received vector, and the remaining terms are corrections to the correlation term.

The Separate Estimation Approach using Gaussian Approximation

As mentioned above, $\boldsymbol{d}_{i,j}$ is a random data symbol drawn from a 2-D constellation on a complex plane with zero mean, i.e., $E[\boldsymbol{d}_{i,j}] = 0$. The variance is the average energy of all constellation points E_{avg}, i.e., $\text{Var}[\boldsymbol{d}_{i,j}] = E_{\text{avg}}$. For MPSK, the M points have equal energy while for QAM they usually don't.

When the number of transmitters n gets larger, we can use central limit theorem to approximate the randomness introduced by the data symbols in $\boldsymbol{t}_i$ and $\boldsymbol{c}_j$, in (4.23) and (4.24), as complex Gaussian random variables

$$\boldsymbol{t}_i \sim \mathcal{CN}(h_1 s_i; \sigma_t^2), \quad (0 \le i \le L-1), \quad \sigma_t^2 = E_{\text{avg}} \sum_{l=2}^{n} |h_l|^2 \tag{4.32}$$

$$\boldsymbol{c}_j \sim \mathcal{CN}(0; \sigma_c^2), \quad (L \le j \le N-1), \quad \sigma_c^2 = E_{\text{avg}} \sum_{l=1}^{n} |h_l|^2 \tag{4.33}$$

Again, the MAP estimation rule leads us to maximize

$$\begin{aligned} S_2^{sa} &= p_{\underline{\boldsymbol{r}}^s}(\underline{r}^s | \boldsymbol{\mu} = \mu) \\ &= (\pi(\sigma^2 + \sigma_t^2))^{-L} (\pi(\sigma^2 + \sigma_c^2))^{-(N-L)} \\ &\quad \cdot \left[\prod_{i=0}^{L-1} e^{-|r_{i+\mu} - h_1 s_i|^2/(\sigma^2+\sigma_t^2)} \right] \left[\prod_{j=L}^{N-1} e^{-|r_{j+\mu}|^2/(\sigma^2+\sigma_c^2)} \right]. \end{aligned} \tag{4.34}$$

Here, we add 'a' to the superscript to indicate this is an approximate approach. After removing all terms independent of μ, we can equivalently maximize

$$S_4^{sa} = \left[\prod_{i=0}^{L-1} e^{(r_{i+\mu} h_1^* s_i^* + r_{i+\mu}^* h_1 s_i - |r_{i+\mu}|^2)/(\sigma^2+\sigma_t^2)} \right] \left[\prod_{j=L}^{N-1} e^{-|r_{j+\mu}|^2/(\sigma^2+\sigma_c^2)} \right] \tag{4.35}$$

Taking the natural logarithms and multiplying by a constant $(\sigma^2 + \sigma_t^2)$, we could

equivalently maximize

$$S_5^{sa} = \sum_{i=0}^{L-1}(r_{i+\mu}h_1^* s_i^* + r_{i+\mu}^* h_1 s_i - |r_{i+\mu}|^2) + \left(\frac{\sigma^2+\sigma_t^2}{\sigma^2+\sigma_c^2}\right)\cdot\sum_{j=L}^{N-1}(-|r_{j+\mu}|^2) \qquad (4.36)$$

Note that $\sum_{j=0}^{N-1}(-|r_{j+\mu}|^2)$ is independent of μ. We can subtract it from the second summation in S_5^{sa} and then obtain

$$S_6^{sa} = \sum_{i=0}^{L-1}(r_{i+\mu}h_1^* s_i^* + r_{i+\mu}^* h_1 s_i) - \left(\frac{\sigma_c^2-\sigma_t^2}{\sigma^2+\sigma_c^2}\right)\cdot\sum_{i=0}^{L-1}|r_{i+\mu}|^2. \qquad (4.37)$$

Note that here $(\sigma_c^2-\sigma_t^2) = E_{\text{avg}}|h_1|^2$. By using Gaussian approximation, we find that the second correction term becomes much simpler when compared with S_6^s in (4.31), while the first correlation term stays the same. For different transmitters, the second correction term is varied, which is proportional to $|h_l|^2$.

The Joint Estimation Approach

Joint estimation of frame positions greatly enlarges the search space to N^n possibilities, which make it unrealistic to be used in practice. Finding an analytic expression for the MAP estimation is complicated or even untractable. However, we may deal with a simplified case involving only 2 transmitters to gain some insights into it and compare its performance with the separate estimation approach.

The MAP rule is to choose the estimate of $(\boldsymbol{\mu_1}, \boldsymbol{\mu_2})$ as $(\mu_1, \mu_2)(0 \le \mu_1, \mu_2 \le N-1)$, such that $S_1^j = \Pr[\boldsymbol{\mu}_1 = \mu_1, \boldsymbol{\mu}_2 = \mu_2 | \underline{\boldsymbol{r}}^j = \underline{r}^j] = p_{\underline{\boldsymbol{r}}^j}(\underline{r}^j | \boldsymbol{\mu}_1 = \mu_1, \boldsymbol{\mu}_2 = \mu_2)\Pr[\boldsymbol{\mu}_1 = \mu_1, \boldsymbol{\mu}_2 = \mu_2]/p_{\underline{\boldsymbol{r}}^j}(\underline{r}^j)$ is maximized. $\Pr[\boldsymbol{\mu}_1 = \mu_1, \boldsymbol{\mu}_2 = \mu_2] = 1/N^2$ for all possible pairs(μ_1, μ_2), we may equivalently search over all possible (μ_1, μ_2) to maximize $S_2^j = p_{\underline{\boldsymbol{r}}^j}(\underline{r}^j | \boldsymbol{\mu}_1 = \mu_1, \boldsymbol{\mu}_2 = \mu_2)$.

There are three possible cases. First, when $\mu_1 = \mu_2$, this goes back to the frame-synchronous case developed in section 4.3.1, with $n = 2$. The corresponding metric

is

$$
\begin{aligned}
S_6^j &= \frac{1}{\sigma^2}\sum_{i=0}^{L-1}(r_{i+\mu}h_1^*s_{1,i}^* + r_{i+\mu}^*h_1s_{1,i} + r_{i+\mu}h_2^*s_{2,i}^* + r_{i+\mu}^*h_2s_{2,i}) \\
&\quad -\frac{1}{\sigma^2}\sum_{i=0}^{L-1}|h_1s_{1,i} + h_2s_{2,i}|^2 \\
&\quad +\sum_{i=L}^{N-1}\left[\ln\left(\sum_{\underline{v}=\underline{v}_1}^{\underline{v}_{M^2}} e^{(\sum_{l=1}^{2}(r_{i+\mu}h_l^*v_l^* + r_{i+\mu}^*h_lv_l) - |\sum_{l=1}^{2}h_lv_l|^2)/\sigma^2}\right)\right].
\end{aligned} \tag{4.38}
$$

Note that compared with the result in section 4.3.1, we have one more term here $-\frac{1}{\sigma^2}\sum_{i=0}^{L-1}|h_1s_{1,i} + h_2s_{2,i}|^2$, because this term is not independent of (μ_1, μ_2) when μ_1 is not equal to μ_2.

In the second case, (μ_1, μ_2) satisfies $0 < |\mu_1 - \mu_2| < L$, which corresponds to the scenario when two sync words have partial overlap. Without any loss of generality, we assume $(0 \le \mu_1 < \mu_2 \le N-1)$, and $\delta \triangleq \mu_2 - \mu_1 (1 \le \delta \le L-1)$. The transmitted symbols within a frame are represented using the elements in a new matrix $\boldsymbol{T}^j$, $\boldsymbol{T}^j =$

$$
\begin{pmatrix}
s_{1,0} & \cdots & s_{1,\delta-1} & s_{1,\delta} & \cdots & s_{1,L-1} & \boldsymbol{d}_{1,L} & \cdots & \boldsymbol{d}_{1,L+\delta-1} & \boldsymbol{d}_{1,L+\delta} & \cdots & \boldsymbol{d}_{1,N-1} \\
\boldsymbol{d}_{2,0} & \cdots & \boldsymbol{d}_{2,\delta-1} & s_{2,0} & \cdots & s_{2,L-\delta-1} & s_{2,L-\delta} & \cdots & s_{2,L-1} & \boldsymbol{d}_{2,L+\delta} & \cdots & \boldsymbol{d}_{2,N-1}
\end{pmatrix}. \tag{4.39}
$$

Note that in our analysis, we implicitly assume $N \ge 2L$. This is a valid assumption in most data transmissions. However, even this assumption isn't true in some cases. The method we use for developing the MAP rule still holds, while the resulting closed-form expression can be different. The received frame without considering the noise and frame shift is

$$
\underline{\boldsymbol{q}}_{1\times N}^j = \underline{h}_{1\times 2}^{\mathrm{T}}\boldsymbol{T}_{2\times N}^j \tag{4.40}
$$

where

$$\begin{aligned} q_i &= h_1 s_{1,i} + h_2 \boldsymbol{d}_{2,i} && (0 \le i \le \delta - 1) \\ q_i &= h_1 s_{1,i} + h_2 s_{2,i-\delta} && (\delta \le i \le L - 1) \\ q_i &= h_1 \boldsymbol{d}_{1,i} + h_2 s_{2,i-\delta} && (L \le i \le L + \delta - 1) \\ q_i &= h_1 \boldsymbol{d}_{1,i} + h_2 \boldsymbol{d}_{2,i} && (L + \delta \le i \le N - 1). \end{aligned} \tag{4.41}$$

Taking the frame shift $\boldsymbol{\mu_1}$ and the additive noise into consideration, the received frame is

$$\underline{\boldsymbol{r}}^j_{1\times N} = \mathrm{T}^{\mu_1}(\underline{\boldsymbol{q}}^j_{1\times N}) + \underline{\boldsymbol{z}}_{1\times N} \tag{4.42}$$

We define the following vector and matrix notations for the random data symbols $\boldsymbol{d}_{i,j}$

$$\begin{aligned} \underline{\boldsymbol{d}}_a &= (\boldsymbol{d}_{2,0}, \boldsymbol{d}_{2,1}, \cdots, \boldsymbol{d}_{2,\delta-1}) \\ \underline{\boldsymbol{d}}_b &= (\boldsymbol{d}_{1,L}, \boldsymbol{d}_{1,L+1}, \cdots, \boldsymbol{d}_{1,L+\delta-1}) \\ \boldsymbol{D}_c &= \begin{pmatrix} \boldsymbol{d}_{1,L+\delta} & \boldsymbol{d}_{1,L+\delta+1} & \cdots & \boldsymbol{d}_{1,N-1} \\ \boldsymbol{d}_{2,L+\delta} & \boldsymbol{d}_{2,L+\delta+1} & \cdots & \boldsymbol{d}_{2,N-1} \end{pmatrix}. \end{aligned} \tag{4.43}$$

Then, we could equivalently maximize

$$S_3^j = \sum_{\text{all}\underline{\boldsymbol{d}}_a} \sum_{\text{all}\underline{\boldsymbol{d}}_b} \sum_{\text{all}\boldsymbol{D}_c} p_{\underline{\boldsymbol{z}}}(\underline{r}^j - \mathrm{T}^{\mu_1}(\underline{q}^j)). \tag{4.44}$$

$\underline{\boldsymbol{z}}$ is complex Gaussian distributed, we have

$$\begin{aligned} p_{\underline{\boldsymbol{z}}}(\underline{r}^j - \mathrm{T}^{\mu_1}(\underline{q}^j)) &= (\pi\sigma^2)^{-N} \left[\prod_{i=0}^{\delta-1} e^{-|r_{i+\mu_1} - h_1 s_{1,i} - h_2 d_{2,i}|^2/\sigma^2} \right] \\ &\quad \cdot \left[\prod_{i=\delta}^{L-1} e^{-|r_{i+\mu_1} - h_1 s_{1,i} - h_2 s_{2,i-\delta}|^2/\sigma^2} \right] \\ &\quad \cdot \left[\prod_{i=L}^{L+\delta-1} e^{-|r_{i+\mu_1} - h_1 d_{1,i} - h_2 s_{2,i-\delta}|^2/\sigma^2} \right] \\ &\quad \cdot \left[\prod_{i=L+\delta}^{N-1} e^{-|r_{i+\mu_1} - h_1 d_{1,i} - h_2 d_{2,i}|^2/\sigma^2} \right] \end{aligned} \tag{4.45}$$

Substituting $p_{\underline{z}}(\underline{r}^j - \mathrm{T}^{\mu_1}(\underline{q}^j))$ into (4.44) and remove all terms independent of (μ_1, μ_2), we can equivalently maximize

$$
\begin{aligned}
S_4^j \;=\; & \left[\prod_{i=\delta}^{L-1} e^{(r_{i+\mu_1}(h_1^* s_{1,i}^* + h_2^* s_{2,i-\delta}^*) + r_{i+\mu_1}^*(h_1 s_{1,i} + h_2 s_{2,i-\delta}) - |h_1 s_{1,i} + h_2 s_{2,i-\delta}|^2)/\sigma^2}\right] \\
& \cdot \left[\prod_{i=0}^{\delta-1} \left(e^{(r_{i+\mu_1} h_1^* s_{1,i}^* + r_{i+\mu_1}^* h_1 s_{1,i})/\sigma^2} \sum_{w=w_1}^{w_M} e^{((r_{i+\mu_1} h_2^* w^* + r_{i+\mu_1}^* h_2 w) - |h_1 s_{1,i} + h_2 w|^2)/\sigma^2} \right)\right] \\
& \cdot \left[\prod_{i=L}^{L+\delta-1} \left(e^{(r_{i+\mu_1} h_2^* s_{2,i-\delta}^* + r_{i+\mu_1}^* h_2 s_{2,i-\delta})/\sigma^2} \sum_{w=w_1}^{w_M} e^{((r_{i+\mu_1} h_1^* w^* + r_{i+\mu_1}^* h_1 w) - |h_1 w + h_2 s_{2,i-\delta}|^2)/\sigma^2} \right)\right] \\
& \cdot \left[\prod_{i=L+\delta}^{N-1} \left(\sum_{\underline{v}=\underline{v}_1}^{\underline{v}_{M^2}} e^{(r_{i+\mu_1}(h_1^* v_1^* + h_2^* v_2^*) + r_{i+\mu_1}^*(h_1 v_1 + h_2 v_2) - |h_1 v_1 + h_2 v_2|^2)/\sigma^2} \right)\right]. \qquad (4.46)
\end{aligned}
$$

Taking the logarithms, we can equivalently maximize

$$
\begin{aligned}
S_5^j \;=\; & \frac{1}{\sigma^2} \sum_{i=0}^{L-1} ((r_{i+\mu_1} h_1^* s_{1,i}^* + r_{i+\mu_1}^* h_1 s_{1,i}) + (r_{i+\mu_1+\delta} h_2^* s_{2,i}^* + r_{i+\mu_1+\delta}^* h_2 s_{2,i})) \\
& - \frac{1}{\sigma^2} \sum_{i=\delta}^{L-1} |h_1 s_{1,i} + h_2 s_{2,i-\delta}|^2 \\
& + \sum_{i=0}^{\delta-1} \left[\ln \left(\sum_{w=w_1}^{w_M} e^{((r_{i+\mu_1} h_2^* w^* + r_{i+\mu_1}^* h_2 w) - |h_1 s_{1,i} + h_2 w|^2)/\sigma^2} \right)\right] \\
& + \sum_{i=L}^{L+\delta-1} \left[\ln \left(\sum_{w=w_1}^{w_M} e^{((r_{i+\mu_1} h_1^* w^* + r_{i+\mu_1}^* h_1 w) - |h_1 w + h_2 s_{2,i-\delta}|^2)/\sigma^2} \right)\right] \\
& + \sum_{i=L+\delta}^{N-1} \left[\ln \left(\sum_{\underline{v}=\underline{v}_1}^{\underline{v}_{M^2}} e^{(r_{i+\mu_1}(h_1^* v_1^* + h_2^* v_2^*) + r_{i+\mu_1}^*(h_1 v_1 + h_2 v_2) - |h_1 v_1 + h_2 v_2|^2)/\sigma^2} \right)\right] \qquad (4.47)
\end{aligned}
$$

Note that, when $\delta = 0$, the result can be simplified to the one for case 1 (4.38).

Next, we consider the case when $|\mu_2 - \mu_1| \geq L$, in which the two sync words have no overlap. Without any loss of generality, we assume $(0 \leq \mu_1 < \mu_2 \leq N-1)$ and

still use δ to denote $\delta = \mu_2 - \mu_1 (L \leq \delta \leq N - L)$. The transmitted matrix is $\boldsymbol{T}^j =$

$$\begin{pmatrix} s_{1,0} & \cdots & s_{1,L-1} & \boldsymbol{d}_{1,L} & \cdots & \boldsymbol{d}_{1,\delta-1} & \boldsymbol{d}_{1,\delta} & \cdots & \boldsymbol{d}_{1,L+\delta-1} & \boldsymbol{d}_{1,L+\delta} & \cdots & \boldsymbol{d}_{1,N-1} \\ \boldsymbol{d}_{2,0} & \cdots & \boldsymbol{d}_{2,L-1} & \boldsymbol{d}_{2,L} & \cdots & \boldsymbol{d}_{2,\delta-1} & s_{2,0} & \cdots & s_{2,L-1} & \boldsymbol{d}_{2,L+\delta} & \cdots & \boldsymbol{d}_{2,N-1} \end{pmatrix}. \tag{4.48}$$

The received frame without considering the noise and frame shift is

$$\underline{\boldsymbol{q}}^j_{1\times N} = \underline{h}^{\mathrm{T}}_{1\times 2} \boldsymbol{T}^j_{2\times N} \tag{4.49}$$

where

$$\begin{aligned} q_i &= h_1 s_{1,i} + h_2 \boldsymbol{d}_{2,i} && (0 \leq i \leq L-1) \\ q_i &= h_1 \boldsymbol{d}_{1,i} + h_2 s_{2,i-\delta} && (\delta \leq i \leq L+\delta-1) \\ q_i &= h_1 \boldsymbol{d}_{1,i} + h_2 \boldsymbol{d}_{2,i} && (L \leq i \leq \delta-1, L+\delta \leq i \leq N-1). \end{aligned} \tag{4.50}$$

Taking the frame shift $\boldsymbol{\mu_1}$ and the additive noise into consideration, the received frame is

$$\underline{\boldsymbol{r}}^j_{1\times N} = \mathrm{T}^{\boldsymbol{\mu}_1}(\underline{\boldsymbol{q}}^j_{1\times N}) + \underline{\boldsymbol{z}}_{1\times N} \tag{4.51}$$

We define the following vector and matrix notations for the random data symbols $\boldsymbol{d}_{i,j}$

$$\begin{aligned} \underline{\boldsymbol{d}}_a &= (\boldsymbol{d}_{2,0}, \boldsymbol{d}_{2,1}, \cdots, \boldsymbol{d}_{2,L-1}) \\ \underline{\boldsymbol{d}}_b &= (\boldsymbol{d}_{1,\delta}, \boldsymbol{d}_{1,\delta+1}, \cdots, \boldsymbol{d}_{1,L+\delta-1}) \\ \boldsymbol{D}_c &= \begin{pmatrix} \boldsymbol{d}_{1,L} & \cdots & \boldsymbol{d}_{1,\delta-1} & \boldsymbol{d}_{1,L+\delta} & \cdots & \boldsymbol{d}_{1,N-1} \\ \boldsymbol{d}_{2,L} & \cdots & \boldsymbol{d}_{2,\delta-1} & \boldsymbol{d}_{2,L+\delta} & \cdots & \boldsymbol{d}_{2,N-1} \end{pmatrix}. \end{aligned} \tag{4.52}$$

We follow the steps derived above and obtain

$$\begin{aligned} p_{\underline{z}}(\underline{r}^j - \mathrm{T}^{\mu_1}(\underline{q}^j)) &= (\pi\sigma^2)^{-N} \left[\prod_{i=0}^{L-1} e^{-|r_{i+\mu_1} - h_1 s_{1,i} - h_2 d_{2,i}|^2/\sigma^2}\right] \\ &\cdot \left[\prod_{i=\delta}^{L+\delta-1} e^{-|r_{i+\mu_1} - h_1 d_{1,i} - h_2 s_{2,i-\delta}|^2/\sigma^2}\right] \\ &\cdot \left[\prod_{L\le i\le \delta-1, L+\delta\le i\le N-1} e^{-|r_{i+\mu_1} - h_1 d_{1,i} - h_2 d_{2,i}|^2/\sigma^2}\right] \end{aligned} \quad (4.53)$$

Substituting $p_{\underline{z}}(\underline{r}^j - \mathrm{T}^{\mu_1}(\underline{q}^j))$ into (4.44) and remove all terms independent of (μ_1, μ_2), we can equivalently maximize

$$\begin{aligned} S_4^j &= \left[\prod_{i=0}^{L-1} \left(e^{(r_{i+\mu_1} h_1^* s_{1,i}^* + r_{i+\mu_1}^* h_1 s_{1,i})/\sigma^2} \sum_{w=w_1}^{w_M} e^{((r_{i+\mu_1} h_2^* w^* + r_{i+\mu_1}^* h_2 w) - |h_1 s_{1,i} + h_2 w|^2)/\sigma^2} \right)\right] \\ &\cdot \left[\prod_{i=\delta}^{L+\delta-1} \left(e^{(r_{i+\mu_1} h_2^* s_{2,i-\delta}^* + r_{i+\mu_1}^* h_2 s_{2,i-\delta})/\sigma^2} \sum_{w=w_1}^{w_M} e^{((r_{i+\mu_1} h_1^* w^* + r_{i+\mu_1}^* h_1 w) - |h_1 w + h_2 s_{2,i-\delta}|^2)/\sigma^2} \right)\right] \\ &\cdot \left[\prod_{L\le i\le \delta-1, L+\delta\le i\le N-1} \left(\sum_{\underline{v}=\underline{v}_1}^{\underline{v}_{M^2}} e^{(r_{i+\mu_1}(h_1^* v_1^* + h_2^* v_2^*) + r_{i+\mu_1}^*(h_1 v_1 + h_2 v_2) - |h_1 v_1 + h_2 v_2|^2)/\sigma^2} \right)\right]. \end{aligned} \quad (4.54)$$

Taking natural logarithms, we can equivalently maximize

$$\begin{aligned} S_5^j &= \frac{1}{\sigma^2} \sum_{i=0}^{L-1} ((r_{i+\mu_1} h_1^* s_{1,i}^* + r_{i+\mu_1}^* h_1 s_{1,i}) + (r_{i+\mu_1+\delta} h_2^* s_{2,i}^* + r_{i+\mu_1+\delta}^* h_2 s_{2,i})) \\ &+ \sum_{i=0}^{L-1} \left[\ln\left(\sum_{w=w_1}^{w_M} e^{((r_{i+\mu_1} h_2^* w^* + r_{i+\mu_1}^* h_2 w) - |h_1 s_{1,i} + h_2 w|^2)/\sigma^2} \right)\right] \\ &+ \sum_{i=\delta}^{L+\delta-1} \left[\ln\left(\sum_{w=w_1}^{w_M} e^{((r_{i+\mu_1} h_1^* w^* + r_{i+\mu_1}^* h_1 w) - |h_1 w + h_2 s_{2,i-\delta}|^2)/\sigma^2} \right)\right] \\ &+ \sum_{L\le i\le \delta-1, L+\delta\le i\le N-1} \left[\ln\left(\sum_{\underline{v}=\underline{v}_1}^{\underline{v}_{M^2}} e^{(r_{i+\mu_1}(h_1^* v_1^* + h_2^* v_2^*) + r_{i+\mu_1}^*(h_1 v_1 + h_2 v_2) - |h_1 v_1 + h_2 v_2|^2)/\sigma^2} \right)\right]. \end{aligned} \quad (4.55)$$

As anticipated, the optimal frame synchronization rule using separate estimation becomes very complicated.

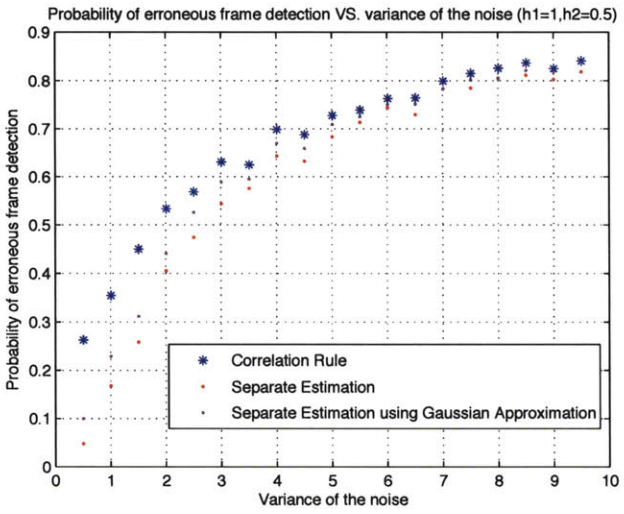

Figure 4-6 – Separate frame detection using the correlation rule, the optimal decision rule and the suboptimal rule using Gaussian approximation in the frame-asynchronous case. Two transmitters use Barker codes, $h_1 = 1$, $h_2 = 0.5$, and noise variance (σ^2) ranges from 0.5 to 9.5

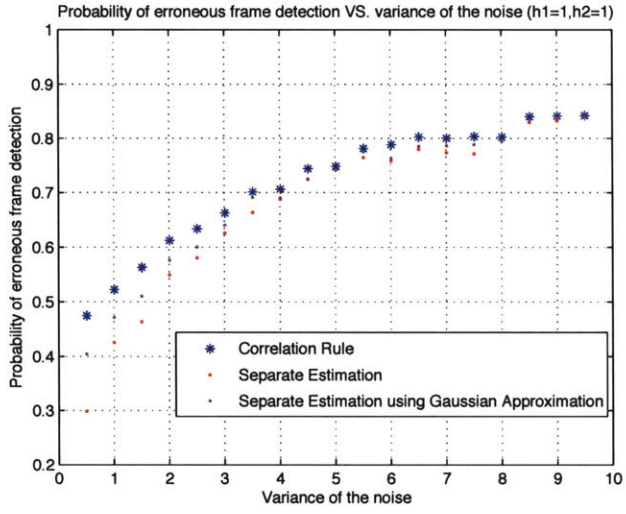

Figure 4-7 – Separate frame detection using the correlation rule, the optimal decision rule and the suboptimal rule using Gaussian approximation in the frame-asynchronous case. Two transmitters use Barker codes, $h_1 = 1$, $h_2 = 1$, and noise variance (σ^2) ranges from 0.5 to 9.5

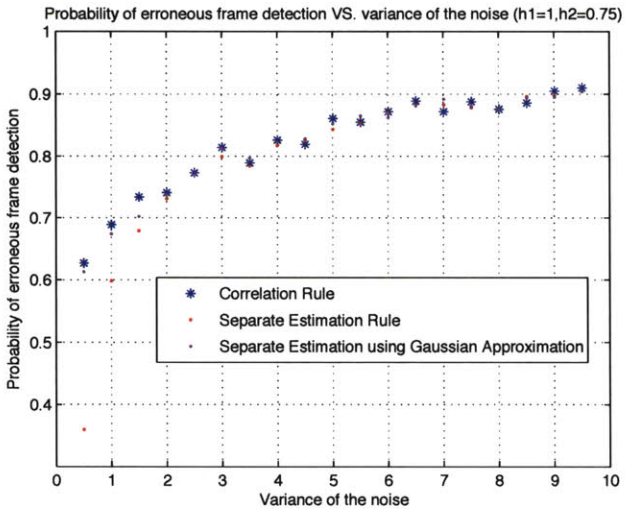

Figure 4-8 – Separate frame detection of transmitter 2's signal using the correlation rule, the optimal decision rule and the suboptimal rule using Gaussian approximation in the frame-asynchronous case. Two transmitters use Barker codes, $h_1 = 1$, $h_2 = 0.75$, and noise variance (σ^2) ranges from 0.5 to 9.5

In Figure.4-6, we show the simulation results for separately estimating frame positions. We estimate the frame position of the data stream sent by transmitter 1 when $h_1 = 1$, $h_2 = 0.5$. In our simulation, we use the same Barker code as the sync-word for transmitter 2 and assume transmitter 2's frame is 10 symbols later than transmitter 1's. As expected, the optimal rule delivers the best performance. The suboptimal rule using Gaussian approximation also outperforms the correlation rule significantly, but not as much as the optimal decision rule. We note that the performance of all three methods degrades very fast as the noise variance increases above 4, with more than 60% of the detections wrong. This observation is more clear in Figure.4-7, where h_2 is also set to 1. The frame detection error rates are much higher than those in Figure.4-6. This is because the sync-words for both transmitters are the same, i.e., the 13-bit Barker code. If the amplification factors h_1 and h_2 are the same, the correlation terms for $\mu = 0$ and $\mu = 10$ are also identical. Therefore, it's more likely to make false detections.

The separate estimation approach doesn't work so well when we do frame detection

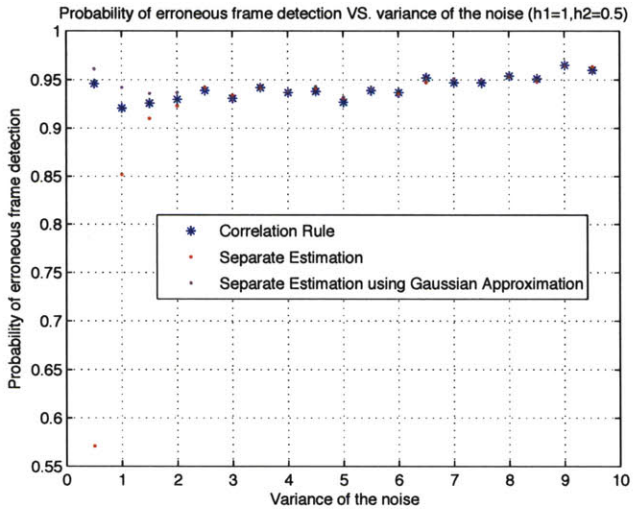

Figure 4-9 – Separate frame detection of transmitter 2's signal using the correlation rule, the optimal decision rule and the suboptimal rule using Gaussian approximation in the frame-asynchronous case. Two transmitters use Barker codes, $h_1 = 1$, $h_2 = 0.5$, and noise variance (σ^2) ranges from 0.5 to 9.5

of the weaker signal, as seen in Figure.4-8 and Figure.4-9. We try to determine the frame location of transmitter 2' signal, when $h_2 = 0.75$ and $h_2 = 0.5$, respectively. For the $h_2 = 0.75$ case, the error detection rates go above 0.6 very quickly and the suboptimal rule using Gaussian approximation works as poorly as the correlation rule. When $h_2 = 0.5$, the decoding performance is totally unacceptable. The reason is quite obvious: the two transmitters are using the same sync-words, the one used by transmitter 1 introduces a very large correlation term at $\mu = 0$. The detector thus usually mistakes $\mu = 0$ as the frame location, which is actually transmitter 1's frame location, and not transmitter 2's. It is interesting to observe that the error detection rate of the optimal decision rule is much lower than those of the other two methods when $\sigma^2 = 0.5$, which is close to 0.5.

It's not wise to use the same sync-words for both transmitters in the frame-asynchronous case. It can be predicted that if we choose a different low-autocorrelation sync-word for transmitter 2, the detection performance can be greatly improved. This is proved by simulation, as seen in Figure.4-10. We use the Neuman-Hofman sequence,

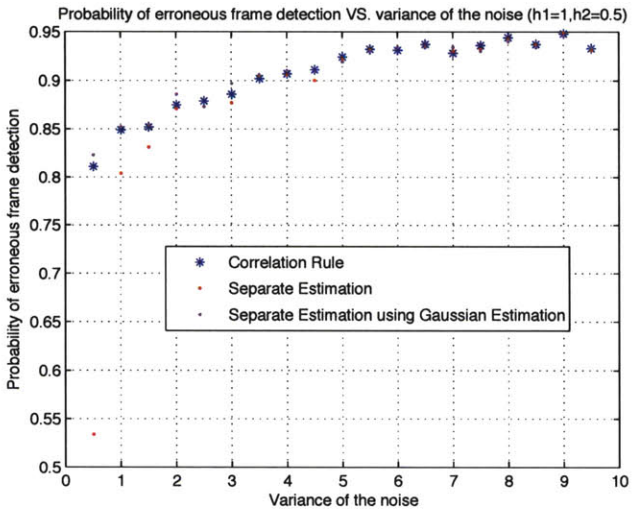

Figure 4-10 – Separate frame detection of transmitter 2's signal using the correlation rule, the optimal decision rule and the suboptimal rule using Gaussian approximation in the frame-asynchronous case. Transmitter 1 uses the Barker code, transmitter 2 uses the Neuman-Hofman code. $h_1 = 1$, $h_2 = 0.5$, and noise variance (σ^2) ranges from 0.5 to 9.5

as introduced in Massey's paper, as the sync-word for transmitter 2 and still set h_2 as 0.5. We observe the performance enhancement compared with Figure.4-9. However, the error detection rates still remain very high. We can conclude that we must be cautious when using separate estimation approachs to do frame synchronization on the weaker signal. A much more reliable approach would be to subtract the stronger signal first and then locate the frame position for the second signal.

Next, we examine how the suboptimal rule using Gaussian approximation performs as the number of transmitters changes. The more transmitters we have, the more accurate the Gaussian approximation is. Figure.4-11 shows the case when three transmitters are considered, $h_1 = 1$, $h_2 = 0.5$, $h_3 = 0.3$. Again, all three transmitters have the same Barker code as the sync-words. We only estimate the frame location of the transmitter 1. As seen from Figure.4-11, the curve for the suboptimal approach using Gaussian approximation stays much closer to that for the optimal decision approach, compared with Figure.4-6. This observation confirms our prediction that as the number of transmitters increases, the performance of the suboptimal detection

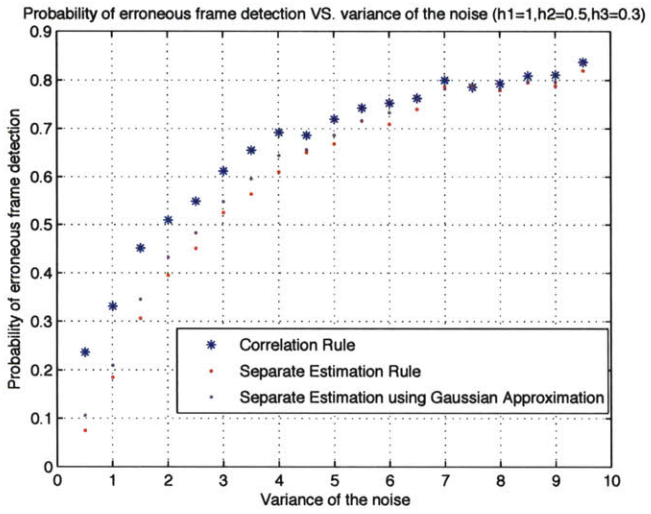

Figure 4-11 – Separate frame detection using the correlation rule, the optimal decision rule and the suboptimal rule using Gaussian approximation in the frame-asynchronous case. Three transmitters use Barker codes, $h_1 = 1$, $h_2 = 0.5$, $h_3 = 0.3$, and noise variance (σ^2) ranges from 0.5 to 9.5

rule using Gaussian approximation converges to that of the optimal decision rule.

Finally, we display in Figure.4-12 the simulation results for the joint estimation approach when $h_1 = 1$,$h_2 = 0.75$. Compared with the separate estimation approach, the joint estimation approach does not demonstrate a significant performance improvement for both stronger and weaker signals. Therefore, it's preferable to use the separate estimation approach in practice after comparing the detection performance and the computational complexity.

4.4 Summary

In this chapter, we derive the optimal decision rules for frame synchronization for MIMO and MAC channels. The results show that conventionally adopted correlation rules for locating the starting symbols of frames are in fact only sub-optimal. The expression should be adjusted with an energy correction term.

The RFID signal separation system introduced in Chapter 3 falls into the category

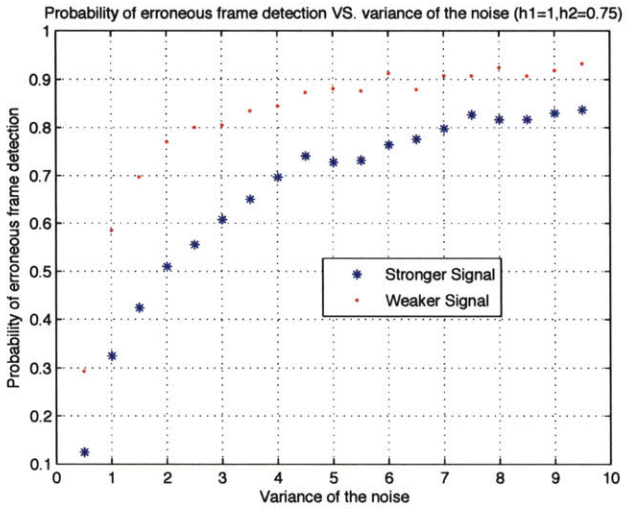

Figure 4-12 – Joint frame detection of both transmitters' signals using the optimal decision rule. Transmitter 1 uses the Barker code, transmitter 2 uses the Neuman-Hofman code. $h_1 = 1$, $h_2 = 0.75$, and noise variance (σ^2) ranges from 0.5 to 9.5

of frame-asynchronous MAC channels, which is the main focus of this chapter. We propose three approaches:separate estimation, separate estimation with Gaussian approximation, and joint estimation. Out of the three methods, the separate estimation with Gaussian approximation gives the simplest and most easily-implementable decision rule, but it is least accurate. The joint estimation algorithm is optimal in theory, but leads to a very complicated decision rule even for the simplest 2-transmitter case. As the number of transmitters increases, the separate estimation rule using Gaussian approximation should be preferable.

Chapter 5

Future Research

In this chapter, we briefly summarize ongoing research work and future directions. Mainly, we are interested in how to achieve signal separation in a more general network context. We would like to investigate two scenarios. First, in the case of no symbol-level synchonization, analog FM signal separation techniques may be applied to separate two continuous-phase FSK signals such as GMSK. Second, many proposed algorithms rely on symbol-level synchronization among multiple transmitters. In a random-access wireless network, it is interesting to consider how to design a coordinating protocol that synchronizes multiple transmitters.

In a random access network, there are greater challenges when pursuing signal separation:

- In a random access network, there is no mechanism to guarantee that multiple transmitters start sending signals in a symbol-aligned manner. This results in algorithms that are based on symbol-synchronization which are hardly applicable.

- All transmitters, together with the receiver, use different oscillators to generate the carrier. Thus, from the receiver's perspective, all signals have different frequency offsets.

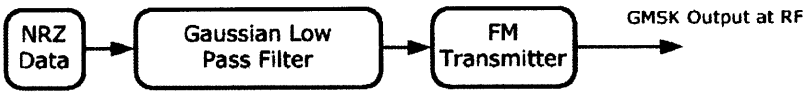

Figure 5-1 – The block diagram of the GMSK transmitter

- A wireless channel may experience severe noise, interference and multipath fading. As a result, a weak design results in a failed system.
- High data rate communications require signal processing in realtime. This disallows an over-convoluted algorithm and expensive computation.

Continuous-Phase Frequency Shift Keying (CPFSK) modulated signals circumvent some of these problems. These waveforms have continuous phase and constant envelope, which we can utilize in separating multiple signals. CPFSK signals can be detected noncoherently, thus alleviating the strict requirement of carrier recovery in coherent detection. Most importantly, CPFSK signals can be treated as ordinary FM analog signals with embedded digital information. Many algorithms for separating FM signals can be utilized to separate the CPFSK signals.

Hamkins developed an analytic technique for analog FM signal separation and we will investigate the opportunity to apply it towards separating two GMSK signals [11]. GMSK is a simple binary modulation scheme, derived from MSK. GMSK is widely used for its excellent power efficiency and spectral efficiency. It's currently used in Global System for Mobile (GSM) system. The easiest way to generate a GMSK signal is to pass a NRZ message binary bit stream through a Gaussian filter, as shown in Figure.5-1.

Note that the last module in the GMSK transmitter is an FM modulator, which clearly shows us that the GMSK signal can be taken as an ordinary FM signal. The GMSK signal can be either detected coherently or noncoherently using standard FM discriminators. Noncoherent detection is suboptimal, but the receiver is much simpler to implement. The block diagram of the complete system for separating two GMSK signals using noncoherent detection is shown in Figure.5-2.

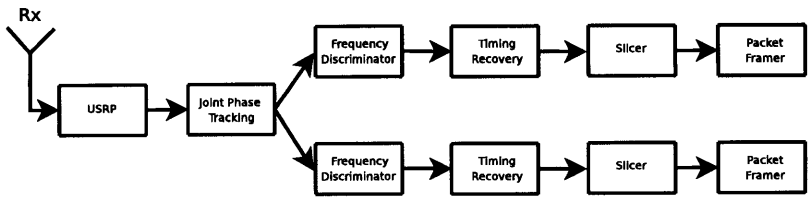

Figure 5-2 – The block diagram of the system for separating two GMSK signals

A significant challenge when implementing signal separation algorithms is that many algorithms assume all signals are symbol-aligned, which is usually an invalid assumption in a random access network. There exists no coordinator for the transmitters so that they may transmit signals simultaneously. For example, one method for separating two co-channel GMSK signals using soft outputs is presented in [14]. However, here, perfect synchronization and channel estimation are assumed. These assumptions make the algorithm very difficult to realize in practice. In future work, we are interesting in designing a protocol that achieves symbol synchronization among transmitters with tolerable timing accuracy.

Chapter 6

Conclusions

Digital signal separation techniques foresee the opportunities to provide greater network throughputs, more enjoyable quality of service to users and better solutions to current network problems. The goal of this research is to 1) find out where and how we can apply signal separation techniques in a real world application, With the multiple RFID cards' reader, signal separation finds an interesting and useful position; and 2) in a general random access network context, implement signal separation algorithms in the software radio system and analyze encountered problems in both theory and practice. We demonstrate our starting efforts by studying GMSK signal separation.

In the first chapter, we introduce the motivation of our research. Signal separation provides us with a new perspective on interference and can potentially improve the performance of the MAC layer protocol and the efficiency of the overall network system significantly.

Chapter 3 documents a complete system design of a multiple RFID card reader. We first analyze the digital waveforms mathematically and then provide a discrete channel model for multiple RFID signals. It is evident that correctly estimating the distinct power levels is the key factor in separating the signals. We show that accurate estimation can be performed by using peak detection of the histogram of the received samples. We also show that selecting a correct phase θ_0 is crucial in power level

detection. The complete block diagram of the system is shown at the end with a graphical interface.

Chapter 4 is the study of an interesting and important problem arising from the multiple RFID cards' reader called optimum frame synchronization. Our derivation proves that the conventionally used correlation rule for locating the position of the sync word is in fact not optimal. We obtain the optimum detection rules for the MIMO channel, and the MAC channel, which is still missing in this area of research. For the MAC channel, which is also the channel for the multiple RFID cards, we develop three different rules. The joint estimation approach gives the optimal criteria, but leads to unaffordable complexity. The separate estimation with Gaussian approximation provides a clear form of decision rule.

In Chapter 5, we briefly introduce our ongoing research work and future extensions. Several other important issues have been left for future work. Many of the results of this thesis could be extended. For the multiple RFID cards' reader, we can use time diversity combining to improve the decoding performance. When the number of cards increases, it becomes more sensitive to select the value of ϕ_0 in generating the local cosine wave. Finding the optimal ϕ_0 requires more experiments and testing. As for the GMSK signal separation, we have not had a successful real-time online system working. Some design parameters and decisions need to be further calibrated. More algorithms will be included in the system and tested on the GNU Radio platform in the future.

Appendix A

Amplitude Estimation

As we introduced in Chapter 3, when we separate the signal generated by four RFID cards, we first estimate the 16 distinct power levels created by different combinations of source symbols, $\pm l_8, \pm l_7, \pm l_6, \pm l_5, \pm l_4, \pm l_3, \pm l_2, \pm l_1$, where $l_8 > l_7 > l_6 > l_5 > l_4 > l_3 > l_2 > l_1 > 0$. Then, we estimate the amplitudes of the four RFID signals g_1, g_2, g_3, g_4 by solving a set of linear equations and pick up the one with the smallest square error. We assume $g_1 > g_2 > g_3 > g_4 > 0$. For the four cards' case, there are 14 possible situations depending on the values of g_1, g_2, g_3, g_4, which in turn lead to 14 linear equations to solve. In this appendix, we list all the 14 possibilities and give the corresponding condition for each case

1. $h_1 > h_2 + h_3 + h_4$, $h_2 > h_3 + h_4$

$$\begin{pmatrix} 1 & 1 & 1 & 1 \\ 1 & 1 & 1 & -1 \\ 1 & 1 & -1 & 1 \\ 1 & 1 & -1 & -1 \\ 1 & -1 & 1 & 1 \\ 1 & -1 & 1 & -1 \\ 1 & -1 & -1 & 1 \\ 1 & -1 & -1 & -1 \end{pmatrix} \begin{pmatrix} g_1 \\ g_2 \\ g_3 \\ g_4 \end{pmatrix} = \begin{pmatrix} l_8 \\ l_7 \\ l_6 \\ l_5 \\ l_4 \\ l_3 \\ l_2 \\ l_1 \end{pmatrix}. \tag{A.1}$$

2. $h_1 > h_2 + h_3 + h_4$, $h_2 < h_3 + h_4$

$$\begin{pmatrix} 1 & 1 & 1 & 1 \\ 1 & 1 & 1 & -1 \\ 1 & 1 & -1 & 1 \\ 1 & -1 & 1 & 1 \\ 1 & 1 & -1 & -1 \\ 1 & -1 & 1 & -1 \\ 1 & -1 & -1 & 1 \\ 1 & -1 & -1 & -1 \end{pmatrix} \begin{pmatrix} g_1 \\ g_2 \\ g_3 \\ g_4 \end{pmatrix} = \begin{pmatrix} l_8 \\ l_7 \\ l_6 \\ l_5 \\ l_4 \\ l_3 \\ l_2 \\ l_1 \end{pmatrix}. \tag{A.2}$$

3. $h_1 < h_2 + h_3 + h_4$, $h_1 > h_2 + h_3$, $h_2 > h_3 + h_4$

$$\begin{pmatrix} 1 & 1 & 1 & 1 \\ 1 & 1 & 1 & -1 \\ 1 & 1 & -1 & 1 \\ 1 & 1 & -1 & -1 \\ 1 & -1 & 1 & 1 \\ 1 & -1 & 1 & -1 \\ 1 & -1 & -1 & 1 \\ -1 & 1 & 1 & 1 \end{pmatrix} \begin{pmatrix} g_1 \\ g_2 \\ g_3 \\ g_4 \end{pmatrix} = \begin{pmatrix} l_8 \\ l_7 \\ l_6 \\ l_5 \\ l_4 \\ l_3 \\ l_2 \\ l_1 \end{pmatrix}. \tag{A.3}$$

4. $h_1 < h_2 + h_3 + h_4$, $h_1 > h_2 + h_3$, $h_2 < h_3 + h_4$

$$\begin{pmatrix} 1 & 1 & 1 & 1 \\ 1 & 1 & 1 & -1 \\ 1 & 1 & -1 & 1 \\ 1 & -1 & 1 & 1 \\ 1 & 1 & -1 & -1 \\ 1 & -1 & 1 & -1 \\ 1 & -1 & -1 & 1 \\ -1 & 1 & 1 & 1 \end{pmatrix} \begin{pmatrix} g_1 \\ g_2 \\ g_3 \\ g_4 \end{pmatrix} = \begin{pmatrix} l_8 \\ l_7 \\ l_6 \\ l_5 \\ l_4 \\ l_3 \\ l_2 \\ l_1 \end{pmatrix}. \tag{A.4}$$

5. $h_1 < h_2 + h_3 + h_4$, $h_1 < h_2 + h_3$, $h_1 > h_2 + h_4$, $h_2 > h_3 + h_4$, $h_1 + h_4 > h_2 + h_3$

$$\begin{pmatrix} 1 & 1 & 1 & 1 \\ 1 & 1 & 1 & -1 \\ 1 & 1 & -1 & 1 \\ 1 & 1 & -1 & -1 \\ 1 & -1 & 1 & 1 \\ 1 & -1 & 1 & -1 \\ -1 & 1 & 1 & 1 \\ 1 & -1 & -1 & 1 \end{pmatrix} \begin{pmatrix} g_1 \\ g_2 \\ g_3 \\ g_4 \end{pmatrix} = \begin{pmatrix} l_8 \\ l_7 \\ l_6 \\ l_5 \\ l_4 \\ l_3 \\ l_2 \\ l_1 \end{pmatrix}. \tag{A.5}$$

6. $h_1 < h_2 + h_3 + h_4$, $h_1 < h_2 + h_3$, $h_1 > h_2 + h_4$, $h_2 > h_3 + h_4$, $h_1 + h_4 < h_2 + h_3$

$$\begin{pmatrix} 1 & 1 & 1 & 1 \\ 1 & 1 & 1 & -1 \\ 1 & 1 & -1 & 1 \\ 1 & 1 & -1 & -1 \\ 1 & -1 & 1 & 1 \\ 1 & -1 & 1 & -1 \\ -1 & 1 & 1 & 1 \\ -1 & 1 & 1 & -1 \end{pmatrix} \begin{pmatrix} g_1 \\ g_2 \\ g_3 \\ g_4 \end{pmatrix} = \begin{pmatrix} l_8 \\ l_7 \\ l_6 \\ l_5 \\ l_4 \\ l_3 \\ l_2 \\ l_1 \end{pmatrix}. \tag{A.6}$$

7. $h_1 < h_2 + h_3 + h_4$, $h_1 < h_2 + h_3$, $h_1 > h_2 + h_4$, $h_2 < h_3 + h_4$, $h_1 + h_4 > h_2 + h_3$

$$\begin{pmatrix} 1 & 1 & 1 & 1 \\ 1 & 1 & 1 & -1 \\ 1 & 1 & -1 & 1 \\ 1 & -1 & 1 & 1 \\ 1 & 1 & -1 & -1 \\ 1 & -1 & 1 & -1 \\ -1 & 1 & 1 & 1 \\ 1 & -1 & -1 & 1 \end{pmatrix} \begin{pmatrix} g_1 \\ g_2 \\ g_3 \\ g_4 \end{pmatrix} = \begin{pmatrix} l_8 \\ l_7 \\ l_6 \\ l_5 \\ l_4 \\ l_3 \\ l_2 \\ l_1 \end{pmatrix}. \tag{A.7}$$

8. $h_1 < h_2 + h_3 + h_4$, $h_1 < h_2 + h_3$, $h_1 > h_2 + h_4$, $h_2 < h_3 + h_4$, $h_1 + h_4 < h_2 + h_3$

$$\begin{pmatrix} 1 & 1 & 1 & 1 \\ 1 & 1 & 1 & -1 \\ 1 & 1 & -1 & 1 \\ 1 & -1 & 1 & 1 \\ 1 & 1 & -1 & -1 \\ 1 & -1 & 1 & -1 \\ -1 & 1 & 1 & 1 \\ -1 & 1 & 1 & -1 \end{pmatrix} \begin{pmatrix} g_1 \\ g_2 \\ g_3 \\ g_4 \end{pmatrix} = \begin{pmatrix} l_8 \\ l_7 \\ l_6 \\ l_5 \\ l_4 \\ l_3 \\ l_2 \\ l_1 \end{pmatrix}. \tag{A.8}$$

9. $h_1 < h_2 + h_4$, $h_2 > h_3 + h_4$, $h_1 + h_4 > h_2 + h_3$

$$\begin{pmatrix} 1 & 1 & 1 & 1 \\ 1 & 1 & 1 & -1 \\ 1 & 1 & -1 & 1 \\ 1 & 1 & -1 & -1 \\ 1 & -1 & 1 & 1 \\ -1 & 1 & 1 & 1 \\ 1 & -1 & 1 & -1 \\ 1 & -1 & -1 & 1 \end{pmatrix} \begin{pmatrix} g_1 \\ g_2 \\ g_3 \\ g_4 \end{pmatrix} = \begin{pmatrix} l_8 \\ l_7 \\ l_6 \\ l_5 \\ l_4 \\ l_3 \\ l_2 \\ l_1 \end{pmatrix}. \tag{A.9}$$

10. $h_1 < h_2 + h_4,\ h_2 > h_3 + h_4,\ h_1 + h_4 < h_2 + h_3$

$$\begin{pmatrix} 1 & 1 & 1 & 1 \\ 1 & 1 & 1 & -1 \\ 1 & 1 & -1 & 1 \\ 1 & 1 & -1 & -1 \\ 1 & -1 & 1 & 1 \\ -1 & 1 & 1 & 1 \\ 1 & -1 & 1 & -1 \\ -1 & 1 & 1 & -1 \end{pmatrix} \begin{pmatrix} g_1 \\ g_2 \\ g_3 \\ g_4 \end{pmatrix} = \begin{pmatrix} l_8 \\ l_7 \\ l_6 \\ l_5 \\ l_4 \\ l_3 \\ l_2 \\ l_1 \end{pmatrix}. \tag{A.10}$$

11. $h_1 < h_2 + h_4,\ h_1 > h_3 + h_4,\ h_2 < h_3 + h_4,\ h_1 + h_4 > h_2 + h_3$

$$\begin{pmatrix} 1 & 1 & 1 & 1 \\ 1 & 1 & 1 & -1 \\ 1 & 1 & -1 & 1 \\ 1 & -1 & 1 & 1 \\ 1 & 1 & -1 & -1 \\ -1 & 1 & 1 & 1 \\ 1 & -1 & 1 & -1 \\ 1 & -1 & -1 & 1 \end{pmatrix} \begin{pmatrix} g_1 \\ g_2 \\ g_3 \\ g_4 \end{pmatrix} = \begin{pmatrix} l_8 \\ l_7 \\ l_6 \\ l_5 \\ l_4 \\ l_3 \\ l_2 \\ l_1 \end{pmatrix}. \tag{A.11}$$

12. $h_1 < h_2 + h_4,\ h_1 > h_3 + h_4,\ h_2 < h_3 + h_4,\ h_1 + h_4 < h_2 + h_3$

$$\begin{pmatrix} 1 & 1 & 1 & 1 \\ 1 & 1 & 1 & -1 \\ 1 & 1 & -1 & 1 \\ 1 & -1 & 1 & 1 \\ 1 & 1 & -1 & -1 \\ -1 & 1 & 1 & 1 \\ 1 & -1 & 1 & -1 \\ -1 & 1 & 1 & -1 \end{pmatrix} \begin{pmatrix} g_1 \\ g_2 \\ g_3 \\ g_4 \end{pmatrix} = \begin{pmatrix} l_8 \\ l_7 \\ l_6 \\ l_5 \\ l_4 \\ l_3 \\ l_2 \\ l_1 \end{pmatrix}. \tag{A.12}$$

13. $h_1 < h_3 + h_4,\ h_1 + h_4 > h_2 + h_3$

$$\begin{pmatrix} 1 & 1 & 1 & 1 \\ 1 & 1 & 1 & -1 \\ 1 & 1 & -1 & 1 \\ 1 & -1 & 1 & 1 \\ -1 & 1 & 1 & 1 \\ 1 & 1 & -1 & -1 \\ 1 & -1 & 1 & -1 \\ 1 & -1 & -1 & 1 \end{pmatrix} \begin{pmatrix} g_1 \\ g_2 \\ g_3 \\ g_4 \end{pmatrix} = \begin{pmatrix} l_8 \\ l_7 \\ l_6 \\ l_5 \\ l_4 \\ l_3 \\ l_2 \\ l_1 \end{pmatrix}. \tag{A.13}$$

14. $h_1 < h_3 + h_4$, $h_1 + h_4 < h_2 + h_3$

$$\begin{pmatrix} 1 & 1 & 1 & 1 \\ 1 & 1 & 1 & -1 \\ 1 & 1 & -1 & 1 \\ 1 & -1 & 1 & 1 \\ -1 & 1 & 1 & 1 \\ 1 & 1 & -1 & -1 \\ 1 & -1 & 1 & -1 \\ -1 & 1 & 1 & -1 \end{pmatrix} \begin{pmatrix} g_1 \\ g_2 \\ g_3 \\ g_4 \end{pmatrix} = \begin{pmatrix} l_8 \\ l_7 \\ l_6 \\ l_5 \\ l_4 \\ l_3 \\ l_2 \\ l_1 \end{pmatrix}. \tag{A.14}$$

After solving the 14 sets of linear equations, we should make sure that all the conditions listed above and the basic assumption $g_1 > g_2 > g_3 > g_4 > 0$ are satisfied. Then, we pick up the one with the smallest square error.

Bibliography

[1] Ettus research. http://www.ettus.com/.

[2] *Digital Communications.* McGraw-Hill, 4th edition, August 2000.

[3] B. Arons. A review of the cocktail party effect. *Journal of the American Voice I/O Society*, 12:35–50, July 1992.

[4] Eric Blossom. Exploring Gnu Radio. Online Document, November 2004. http://www.gnu.org/software/gnuradio/doc/exploring-gnuradio.html.

[5] K. Giridhar, S. Chari, J. Shynk, and R. P. Gooch. Joint demodulation of cochannel signals using MLSE and MAPSD algorithms. In *Proc. IEEE International Conference on Acoustics, Speech and Signal Processing*, volume IV, pages 160–163, Minneapolis, MN, April 1993.

[6] K. Giridhar, S. Chari, J. J. Shynk, R. P. Gooch, and D. J. Artman. Joint estimation algorithms for cochannel signal demodulation. In *Proc. IEEE Interational Conference on Communications*, pages 1497–1501, Geneva, Switzerland, May 1993.

[7] K. Giridhar, John J. Shynk, Amit Mathur, Sujai Chari, and Richard P. Gooch. Nonlinear techniques for the joint estimation of cochannel signals. *IEEE Transactions on Communications*, 45(4):473–484, APRIL 1997.

[8] R. Gooch, C. Jorgensen, and M. Ready. The demod-remod technique for demodulating co-channel FSK signals. In *Conference Record of the Twenty-Fifth Asilomar Conference on Signals, Systems and Computers*, November 1991.

[9] R. P. Gooch and B. J. Sublett. Demodulation of co-channel QAM signals. In *Proc. IEEE International Conference on Acoustics, Speech and Signal Processing*, pages 1392–1395, Glasgow, Scotland, May 1989.

[10] S. J. Grant and J. K. Cavers. Multiuser channel estimation for detection of cochannel signals. *IEEE Transactions on Communications*, 2001.

[11] J. Hamkins. An Analytic Technique to Separate Co-channel FM Signals. *IEEE Transactions on Communications*, 48(4):543–546, April 2000.

[12] Brad A. Hedstrom and R. Lynn Kirlin. Co-channel signal separation using coupled digital phase-locked loops. *IEEE Transactions on Communications*, 44(10):1373–1384, October 1996.

[13] C.Richard Johnson Jr. and William A. Sethares. *Telecommunications Breakdown: Concepts of Communication Transmitted via Software-Defined Radio.* Prentice Hall, 2003.

[14] J.Wu and G. Saulnier. Soft output detection of cochannel gmsk signals. In *Military Communications Conference (MILCOM)*, 2003.

[15] J. L. Massey. Optimum frame synchronization. *IEEE Transactions on Communications*, COM-20:115–119, April 1972.

[16] Peter A. Murphy and Gary E. Ford. Co-channel demodulation for continuous-phase modulated signals. In *Proc. Twenty-Ninth Asilomar Conf. Signals, Syst., Comput.*, pages 330–334, Pacific Grove, CA, November 1995.

[17] M.J. Ready and S. Chari. Demodulation of co-channel FSK signals using joint maximum likelihood sequence estimation. In *Conference Record of the Twenty-*

Seventh Asilomar Conference on Signals, Systems and Computers, November 1993.

[18] Lang Tong, Qing Zhao, and Gokhan Mergen. Multipacket reception in random access wireless networks: From signal processing to optimal medium access control. *IEEE Communications Magazine*, pages 108–112, November 2001.

[19] E. S. Warner and I. K. Proudler. Single-channel blind signal separation of filtered MPSK signals. In *Proc. IEE-Radar, Sonar, Navig.*, volume 150, pages 396–402, December 2003.

[20] Grace Woo. Evaluation and implementation of co-channel bpsk source separation. Master's thesis, Massachusetts Institute of Technology, 2007.